Hydrological Processes

Seasonal snow cover decreases fraction of young water in high Alpine catchments

Journal:	*Hydrological Processes*
Manuscript ID	HYP-19-0896.R2
Wiley - Manuscript type:	Special Issue Paper
Date Submitted by the Author:	n/a
Complete List of Authors:	Ceperley, Natalie; University of Lausanne, IDYST; University of Bern, Institute of Geography; University of Bern, Oeschger Center for Climate Change Research Zuecco, Giulia; University of Padova Department of Land Environment Agriculture and Forestry, Department of Land, Environment, Agriculture and Forestry Beria, Harsh; University of Lausanne, IDYST Carturan, Luca; University of Padova Department of Land Environment Agriculture and Forestry, Department of Land, Environment, Agriculture and Forestry; Universita degli studi di Padova Dipartimento di Geoscienze, Department of Geosciences Michelon, Anthony; University of Lausanne, IDYST Penna, Daniele; University of Florence, Department of Agriculture, Food, Environment and Forestry Larsen, Joshua; University of Lausanne, IDYST; University of Birmingham, School of Geography, Earth and Environmental Sciences; University of Birmingham, The Birmingham Institute of Forest Research (BIFoR) Schaefli, Bettina; University of Lausanne, IDYST; University of Bern, Institute of Geography; University of Bern, Oeschger Center for Climate Change Research
Keywords:	snow hydrology, young water fraction, Alpine catchment, snowmelt, degree-day model, water stable isotopes

Keywords: young water fraction, snow hydrology, water stable isotopes, Alpine catchment, snowmelt, degree-day model

Running Title: Snow cover decreases young water fractions

Full Author Names: Natalie Ceperley[1,2,3], Giulia Zuecco[4], Harsh Beria[1], Luca Carturan[4,5], Anthony Michelon[1], Daniele Penna[6], Joshua Larsen[1,7,8], Bettina Schaefli[1,2,3]

[1]Institute of Earth Surface Dynamics, University of Lausanne, Lausanne, Switzerland
[2] Now at: Institute of Geography, University of Bern, Bern, Switzerland
[3]Now at: Oeschger Centre for Climate Change Research, University of Bern, Bern, Switzerland
[4]Department of Land, Environment, Agriculture and Forestry, University of Padova, Italy
[5]Department of Geosciences, University of Padova, Italy
[6]Department of Agriculture, Food, Environment and Forestry, University of Florence, Italy
[7] Now at: School of Geography, Earth and Environmental Sciences, University of Birmingham, United Kingdom
[8] Now at: The Birmingham Institute of Forest Research (BIFoR), University of Birmingham, United Kingdom

Correspondence to:

Natalie Ceperley, natalie.ceperley@giub.unibe.ch, Institute of Geography, University of Bern Hallerstrasse 12, 3012 Bern, Switzerland

Acknowledgements:

The work of HB, NC, AM and BS was funded by the Swiss National Science Foundation (SNSF), grant number PP00P2_157611. GZ acknowledges the financial support provided by Fondazione Cassa di Risparmio di Padova e Rovigo (Italy) (research project "Ecohydrological Dynamics and Water Pathways in Forested Catchments", Bando Starting Grants 2015) and DOR2019 (research project "Analisi dei processi di generazione di deflusso in bacini d'alta quota", University of Padova, Italy). We thank Marco Borga for providing comments on an earlier version of the manuscript.

This paper proposes a framework to quantify the young water fraction of streamflow (F_{YW}) in snow dominated catchments based on stable water isotopes and a simple snow accumulation model. Based on three case studies from the Alps, the challenges and pitfalls of F_{YW} estimation in presence of seasonal snow cover are discussed, with ensuing recommendations for best practices. The results confirm previous findings that seasonal snow cover leads to low F_{YW} .

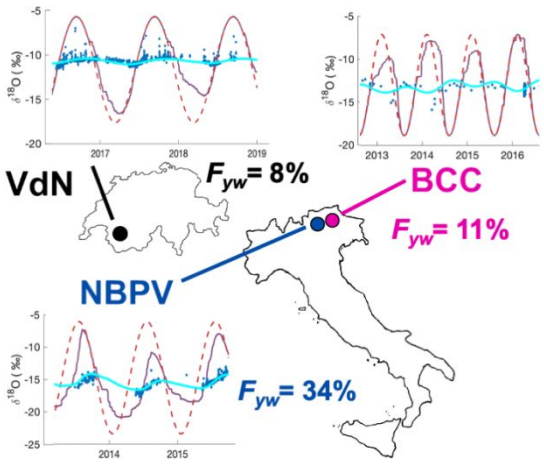

Seasonal snow cover decreases young water fractions in high Alpine catchments

Natalie Ceperley, Giulia Zuecco, Harsh Beria, Luca Carturan, Anthony Michelon, Daniele Penna, Joshua Larsen, Bettina Schaefli

Seasonal snow cover decreases young water fractions in high Alpine catchments

Natalie Ceperley[1,2,3], Giulia Zuecco[4], Harsh Beria[1], Luca Carturan[4,5], Anthony Michelon[1], Daniele Penna[6], Joshua Larsen[1,7,8], Bettina Schaefli[1,2,3]

[1]Institute of Earth Surface Dynamics, University of Lausanne, Lausanne, Switzerland
[2] Now at: Institute of Geography, University of Bern, Bern, Switzerland
[3]Now at: Oeschger Centre for Climate Change Research, University of Bern, Bern, Switzerland
[4]Department of Land, Environment, Agriculture and Forestry, University of Padova, Italy
[5]Department of Geosciences, University of Padova, Italy
[6]Department of Agriculture, Food, Environment and Forestry, University of Florence, Italy
[7] Now at: School of Geography, Earth and Environmental Sciences, University of Birmingham, United Kingdom
[8] Now at: The Birmingham Institute of Forest Research (BIFoR), University of Birmingham, United Kingdom

Correspondence to:

Natalie Ceperley, natalie.ceperley@giub.unibe.ch, Institute of Geography, University of Bern
Hallerstrasse 12, 3012 Bern, Switzerland

Abstract

Estimation of young water fractions (F_{yw}), defined as the fraction of water in a stream younger than approximately 2 – 3 months, provides key information for water resource management in catchments where runoff is dominated by snowmelt. Knowing the average dependence of summer flow on winter precipitation is essential context for comparing regional drought severity and provides the hydrological template for downstream water users and ecosystems. However, F_{yw} estimation based on seasonal signals of stable isotopes of oxygen and hydrogen has not yet explicitly addressed how to parsimoniously include the seasonal shift of water input from snow. Using experimental data from three high-elevation, Alpine catchments (one dominated by glacier and two by snow), we propose a framework to explicitly include the delays induced by snow storage into estimates of F_{yw}. Scrutinizing the key methodological choices when estimating F_{yw} from isotope data, we find that the methods used to construct precipitation input signals from sparse isotope samples can significantly impact F_{yw}. Given this sensitivity, our revised procedure estimates a distribution of F_{yw} values that incorporates a wide range of possible methodological choices and their uncertainties; it furthermore compares the commonly used amplitude ratio approach to a direct convolution approach, which circumvents the assumption that the isotopic signals have a sine curve shape, an assumption that is generally violated in snow dominated environments. Our new estimates confirm that high-elevation Alpine catchments have low F_{yw} values, spanning from 8 to 11%. Such low values have previously been interpreted as the impact of seasonal snow storage alone, but our comparison of different F_{yw} estimation methods suggests that these low F_{yw} values result from a combination of both snow cover effects and longer storage in the subsurface. In contrast, in the highest elevation, glacier dominated catchment, F_{yw} is 3-4 times greater compared to the other two catchments, due to the lower storage and faster drainage processes. A future challenge remains capturing spatio-temporal snowmelt isotope signals during winter baseflow and the snowmelt period remains in order to improve constraints on the F_{yw} estimation technique.

Keywords: young water fraction, snow hydrology, water stable isotopes, Alpine catchment, snowmelt, degree-day model

1 Introduction

Alpine catchments provide freshwater sources to a large fraction of the global population and ecosystems (Viviroli, Durr, Messerli, Meybeck, & Weingartner, 2007). Ecological processes in Alpine river corridors and the water resources supplied from them rely on the annual cycle of snow accumulation and melt, which produces high flows during spring and early summer and low flows during winter (Santos, Portela, Rinaldo, & Schaefli, 2018). Accordingly, the hydrological cycle in such settings is highly sensitive to winter season warming, which can also be amplified with increasing elevations (Huss et al., 2017). High-elevation, Alpine environments are already experiencing such changes, with the Swiss Alps witnessing an increase in air temperatures between 0.25°C and 0.35°C per decade since 1981 (Pepin et al., 2015). It is thus imperative to understand how the Alpine water resources will evolve in a warming climate.

However, our understanding of water resource alteration under changing climate conditions is still hampered by a lack of knowledge regarding actual flow paths and water partitioning in snow dominated, high-elevation, Alpine environments, which require more detailed process-based studies (e.g. Dahlke, Lyon, Jansson, Karlin, & Rosqvist, 2014; Engel et al., 2016; Ohlanders, Rodriguez, & McPhee, 2013; Penna et al., 2014; Schmieder, Garvelmann, Marke, & Strasser, 2018; Zuecco, Carturan, et al., 2019). These flow paths and partitions are not clear, mostly because the processes governing fate of spring snowmelt remain poorly understood (Fang et al., 2019). In particular, it is unclear, over multi-year timescales, how rapidly snowmelt enters the stream versus how long snowmelt may reside in subsurface storage with a slower release back to the stream network.

Stable isotopes of hydrogen and oxygen in water have been shown to provide a set of powerful tools to analyze water flow paths, to estimate the contribution of various end-members to stream runoff (Beria, Larsen, Michelon, Ceperley, & Schaefli, 2020; Penna, Engel, Bertoldi, & Comiti, 2017; Sprenger, Leistert, Gimbel, & Weiler, 2016) and to determine associated water ages (Benettin et al., 2017; Sprenger, Tetzlaff, Buttle, Laudon, & Soulsby, 2018). The majority of tracer-based transit time estimation methods can be most easily categorized into two fundamentally different approaches, although we acknowledge others exist (Kirchner, 2019): i) age distribution estimation based on continuous simulation of rainfall-runoff processes (Rinaldo et al., 2015), and ii) estimation of fractions of young water (F_{yw}) based on the analysis of seasonal tracer signals (Kirchner, 2016a, 2016b). This relatively recent concept has been introduced by Kirchner (2016a, 2016b) to overcome biases associated with transit time estimation.

Process-based rainfall-runoff models quantify the age of streamflow either by flux tracking in completely or partially mixed, but spatially distributed subsurface stores (Birkel, Soulsby, & Tetzlaff, 2015; Douinot et al., 2019) or by coupling spatially-explicit water flux simulations with (calibrated) catchment-scale StorAge selection functions (Rinaldo et al., 2015) that yield streamflow age distributions (Benettin et al., 2017; Fang et al., 2019). The explicit inclusion of snow isotope fractionation processes are rare in such approaches, however they are starting to emerge for applications in high latitude, but not necessarily Alpine, environments (Ala-aho, Tetzlaff, McNamara, Laudon, & Soulsby, 2017; Piovano et al., 2018; Smith, Tetzlaff, Laudon, Maneta, & Soulsby, 2019).

In terms of the second approach to estimate tracer-based water age, F_{yw} estimation is built on seasonal tracer observations in precipitation and streamflow without continuous rainfall-runoff simulations (Kirchner, 2016a, 2016b). F_{yw}, typically defined as the fraction of water less than 1.5-3 months old (Jasechko, Kirchner, Welker, & McDonnell, 2016; Kirchner, 2016b), can be reliably estimated from the dampening of a tracer input signal (total precipitation) to the tracer output signal (streamflow), assuming

that both signals exhibit a sinusoidal pattern at the annual scale that can be estimated from the observed data. The key assumption of these approaches is that precipitation measurements adequately represent the entire liquid water input to the system. This assumption is potentially problematic in Alpine and high latitude catchments where a large fraction of incoming total precipitation can be stored in a seasonal snowpack, with snowpack development not only delaying water supply, but also modifying the isotopic composition of meltwater due to fractionating processes, namely due to sublimation and vapor exchange (Beria et al., 2018). This paper seeks to improve some of these shortcomings in applying F_{yw} estimation to snow dominated Alpine catchments.

Few studies have investigated the potential impact of snow and snowmelt processes on F_{yw} estimates. von Freyberg, Allen, Seeger, Weiler, and Kirchner (2018) used the outputs of an energy-balance snow model to transform observed precipitation quantities into rainfall and melt water; the total precipitation isotope signal was obtained by interpolation from long-term observation networks of isotopes in precipitation (Swiss, Global, and Austrian). This study found low F_{yw} values for snow dominated Alpine catchments and no marked effect on F_{yw} when accounting for the effect of snowmelt (von Freyberg et al., 2018). Fang et al. (2019) used StorAge selection functions in a snow dominated headwater catchment in Colorado and reported higher F_{yw} during periods of high snowmelt. Schmieder et al. (2018) used a surface energy-balance model along with a lumped transit time model in a glacierized catchment in the Austrian Alps and showed that, contrary to the results of von Freyberg et al. (2018), inclusion of snowmelt reduced the amplitude of the input isotope signal, thereby increasing the estimates of F_{yw}.

The purpose of this paper is to build on the foundation of Kirchner (2016b) and provide an easily transferable modelling framework for the estimation of F_{yw} in snow dominated Alpine environments. At the heart of this framework is the computation of the isotopic signal of what we define "equivalent precipitation", P_{eq}, which is the sum of both catchment-scale rainfall and water outflow of the snowpack (e.g. Schaefli et al., 2014). We propose a simple snow accumulation and melt model for the computation of P_{eq} and a parsimonious model of snowpack isotope outflow (Beria et al., 2020). Using P_{eq} (see Section 2.1), we examine the implications of different methodological choices in estimating F_{yw}, in particular i) the construction of the precipitation input signal from sparse isotope samples via weighting and date assignment (see Section 2.3) and ii) the use of either the direct convolution or the amplitude ratio approach in the estimation of F_{yw}, with P_{eq} as the input signal (Section 2.4). We then analyze the effect of accounting explicitly for snowmelt in the input signal on F_{yw} estimates. Our procedure thus provides a distribution of F_{yw} estimates that accounts for the entirety of these potential methodological choices and uncertainties. Moreover, our approach removes the potential confusion associated with defining the input timing as being whenever precipitation falls, regardless of the phase (snow or rain) (von Freyberg et al., 2018). Our sequential methodology is then applied to three climatologically distinct study catchments, one in the Swiss and two in the Italian Alps, each with extensive isotope and hydrological datasets (Section 3).

2 Methods

2.1 Estimation of equivalent precipitation input signals in snow dominated systems

2.1.1 Snow accumulation and melt model

To aid the reader, a full list of abbreviated terms and variables is provided in Appendix B. We begin by addressing the transformation of precipitation and snowmelt input time-series (C_P) into a combined isotope time-series of what we call here equivalent precipitation (P_{eq}), which is the liquid water

immediately available as input to the catchment and for partitioning into subsurface storages or overland flow, and has the isotope composition C_{Peq}.

Estimating C_{Peq} involves the following steps: simulation of i) snowpack accumulation, ii) snowmelt and iii) of isotopic values released during snowmelt. Snow accumulation is simulated with a linear transition between liquid and solid precipitation as a function of air temperature (Harpold et al., 2017): all precipitation falls as snow at temperatures below a minimum threshold (T_{crit1}) and as rain at temperatures above a maximum threshold (T_{crit2}), based on Hock (2003).

Snowmelt is simulated with a degree-day-based melt model (Schaefli et al., 2014); such snow models are known to provide reliable estimates of catchment-scale snowmelt at daily time steps (Hock, 2003; Rango & Martinec, 1995) in environments where melt is largely driven by latent heat transfers (Ohmura, 2001), which is generally the case in Alpine environments. The accumulated snow begins to melt when air temperature rises above a given temperature threshold, T_0 (set to 0°C):

$$M(t) = \begin{cases} \max\left[\zeta(T(t) - T_0), h_S(t)\right], & \text{if } T(t) > T_0 \\ 0 & \text{otherwise} \end{cases}, \quad (1)$$

where $M(t)$ [mm/d] is the daily snowmelt, ζ [mm/°C/d] is the degree-day factor and $h_S(t)$ is the snow water equivalent [mm w.e.] at time t. P_{eq} is then computed as:

$$P_{eq}(t) = M(t) + P_R(t), \quad (2)$$

where $P_R(t)$ is rainfall at time t. The snow model is initialized from the beginning of the hydrological year (1st October) by setting h_S to 0.

To account for elevation gradients, we use an elevation band approach (e.g. Schaefli, Hingray, Niggli, & Musy, 2005): snow accumulation and melt are computed per elevation band and then they are area-weighted. Air temperature is linearly interpolated to mean band elevation with a constant temperature lapse rate per study catchment (see Section 3), whereas precipitation is kept constant. The catchment-scale P_{eq} is obtained from the area-weighted mean.

2.1.2 Snow isotope model

The isotopic composition of snowmelt (C_S) is computed assuming that the water in the snowpack is fully mixed, which is a rough approximation during early snowmelt or intermittent snowpack events (Rücker, Boss, Kirchner, & von Freyberg, 2019), but which is a better approximation for seasonal snowpack during the peak snowmelt season when the snowpack is isothermal (Beria et al., 2018), and has been validated with snow lysimeter data (Ala-Aho, Tetzlaff, McNamara, Laudon, Kormos, et al., 2017). We furthermore assume that any rainfall on a pre-existing snowpack also mixes with the water stored in the snowpack. Under this assumption, the isotopic composition of the snowpack is computed based on the following mass balance:

$$\frac{d(h_S(t)C_S(t))}{dt} = C_{P-fit}P(t) - C_S(t)(P_{eq}(t)), \quad (3)$$

where C_P is the time-series of precipitation isotopic composition, generally, and C_{P-fit} is taken as the sine curve fitted to observations. In this formulation, all rainfall mixing with an existing snowpack is

assumed to exit during the same time step and neglects any water holding capacity of the snowpack or temporary refreezing (e.g. Schaefli et al., 2014).

$C_s(t)$, is then simulated via explicit time stepping with the following initialization $C_s(t_o) = C_{P-fit}(t_o)$.

$C_{Peq}$is obtained as:

$$C_{\mathrm{Peq}}(t) = \frac{1}{a}\left\{\sum_{i=1}^{m} a_{s,i} C_s(P_r(t) + M(t)) + \sum_{j=1}^{n} a_{r,j} C_{P-fit} P_r(t)\right\}, \quad (4)$$

where $a_{s,i}$ is the area of the snow-covered elevation band *i*, $a_{r,j}$ is the area of the non-snow-covered (i.e. receiving rainfall) elevation band *j* and *a* is the total catchment area. From available data at the studied catchments (see Sections 3.1, 3.2, and 3.3.) and nearby sites, no consistent lapse rate in isotopic composition in either rain or snow could be established (Zuecco, Carturan, et al., 2019), thus none is implemented here.

2.1.3 Snow model parameter estimation

The snowpack model has three case-study specific parameters: T_{crit1} and T_{crit2}, the lower and upper thresholds, for snowfall occurrence and ζ, the degree-day factor for snowmelt. These parameters are ideally calibrated based on direct field observations of snowfall (P_s) and of snowmelt (e.g. from snow lysimeters). Such data are however rarely available. Here, we select these parameters based on the reproduction of snow-covered area (SCA) observations (e.g. He, Parajka, Tian, & Bloschl, 2014) or of snow cover duration and based on a parameter sensitivity analysis (Section 4.1).

2.2 Theoretical background: F_{yw} estimation in rainfall dominated systems

Knowing that stable water isotopes of precipitation show typical seasonal cycles in-line with the seasonal cycle in air temperature, Kirchner (2016b) proposed a simple method to quantify F_{yw} in streamflow, which is defined as:

$$F_{\mathrm{yw}} := P_{\mathrm{X}}(X \leq x_{\mathrm{yw}}), \quad (5)$$

where *X* is the streamflow age, P_X is the probability distribution of *X* (i.e. the transit time distribution) and x_{yw} is the threshold age to define young water. Following Kirchner (2016b), this F_{yw} can be closely approximated by the amplitude ratio of seasonal sine curves, C_P and C_Q, fitted to isotope measurements, in this case $\delta^{18}O$, in precipitation ($C_{P\text{-obs}}$) and streamflow ($C_{Q\text{-obs}}$), i.e.

$$F_{\mathrm{yw}} \approx \frac{A_{\mathrm{Q}}}{A_{\mathrm{P}}}, \quad (6)$$

where A_P and A_Q are the amplitudes of the sine curves fitted to $C_{P\text{-obs}}$ and $C_{Q\text{-obs}}$, respectively, resulting in $F_{yw,P}$. We refer to this method as the "amplitude ratio approach". Note that we avoid the subscript *s* for streamflow used in the original formulation of Kirchner (2016b) since in this paper we reserve the symbol *s* for snow. The exact age threshold, x_{yw}, depends on the assumed shape of the catchment transit time distribution, which can vary between 2.3±0.8 months for a wide range of transit time distribution shapes (Kirchner, 2016b). As discussed by Kirchner (2016b), the utility of F_{yw} as a catchment water age metric lays in its relatively low sensitivity to the assumed transit time distribution.

F_{yw} has emerged as a useful alternative to the popular mean transit time, a concept that was shown to suffer from potentially large aggregation biases (Kirchner, 2016b). Such biases commonly occur in heterogeneous catchments because of the aggregation of local transit time distributions with very different parameters (Kirchner, 2016b). In contrast, F_{yw} is largely free of such aggregation biases.

It is, however, useful to recall that in the above F_{yw} estimation framework, the amplitude dampening from A_P to A_Q arises from the convolution of the isotopic input signal C_P with a transit time distribution to yield C_Q (Kirchner, 2016b). Such a convolution approach is classically used in hydrological and groundwater studies to model isotopic output signals (Małoszewski & Zuber, 1982; McGuire & McDonnell, 2006). It was, however, Kirchner (2016a, 2016b) who recognized the potential of the signal dampening as a powerful water age metric for catchment hydrology. Accordingly, we can also use the classical convolution approach to estimate A_Q/A_P.

We compute the convolution of the input signal with the transit time distribution by multiplication in the Fourier domain. This requires a known functional form of the Fourier transform of the transit time distribution. This is notably the case for the often-used Gamma distribution (Kirchner, 2016b), which has the following Fourier transform (Walck, 2007):

$$H(f) = (1 - i2\pi f\beta)^{-\alpha} = (1 - i2\pi f {}^{\overline{\tau}}/_{\alpha})^{-\alpha}, \quad (7)$$

where *H(f)* is the Fourier transform of the Gamma distribution, α is the shape factor and β the scale factor of the Gamma distribution and $\overline{\tau}$ the mean transit time.

Knowing *H(f),* we can use an inverse modelling approach to infer the parameters α and β of a transit time distribution that, if convolved with the input signal, C_P, reproduces as closely as possible the output signal C_Q. Following this parameter optimization step, F_{yw} can be computed directly from the inferred transit time distribution with Eq. 5.

In this paper, we refer to this alternative method to estimate F_{yw} as the "convolution approach". We make no assumption about the functional form of the input and output signals, but conversely assume the functional form of the transit time distribution. We use the Gamma distribution, which can be linked to a wide range of mixing hypotheses (Amin & Campana, 1996), but other distribution functions are possible (Hrachowitz et al., 2016; McGuire & McDonnell, 2006). We furthermore have to choose a distance metric and an optimization algorithm to identify the parameters of the transit time distribution that give the best fit between the observed output signal ($C_{Q\text{-}Obs}$) and the modelled output signal ($C_{Q\text{-}Conv}$, for these details, see Appendix A).

It is important to recall that we should not interpret the inferred transit time distribution (which is subject to aggregation biases, Kirchner, 2016b); and thus, we only use this information to compute F_{yw} from Eq. 5. Although the convolution approach was already discussed in the work of Kirchner (2016b), it has not been further explored in subsequent studies, and in this study, we therefore discuss the opportunities and drawbacks provided by this method in great detail.

2.3 Constructing input and output signals from irregular isotope samples

A key challenge in estimating F_{yw} is the calculation of appropriate isotopic input and output signals based on samples taken at irregular time intervals, usually due to sampling constraints, which can be particularly acute in high-elevation, Alpine catchments due to the difficulty of year-round access to the catchments.

In this study, we explore how to construct continuous time-series of precipitation isotopes based on different options for volume weighting, for date assignment of composite rain or snow samples and for integrating multiple spatial snow samples from the same day.

Volume weighting is required to account for differences of precipitation or streamflow volume associated with each sample (von Freyberg et al., 2018). For streamflow isotopes, we weight all samples by the streamflow measured at the moment of sampling. Similarly, to model the C_{Peq} isotope composition, we weight all simulated values by the simulated P_{eq} amount during the same time step.

For rain and snow, combining observed samples to obtain a time series can be difficult. For instance, the collected samples could be biased by time periods of different durations (e.g., for bulk precipitation versus direct sampling) and of specific portions of a catchment (e.g., only low elevations), or if weighted by precipitation depth, then by measurement location and accuracy. All weighting options tested and applied to construct C_P are summarized in Table 1.

As a first step, we acknowledge that sample collection can be inadequate or even impossible during winter field conditions. The different weighting options for snow are given because most snow samples are in fact not direct samples of snowfall but indirect samples of accumulated snowpack, a necessary substitution where sampling snow when it falls is extremely difficult. Given that sublimation is generally low in Alpine catchments lying mostly above the tree line (Strasser, Bernhardt, Weber, Liston, & Mauser, 2008), average isotope values from snowpack samples should reflect the original snowfall, although temporal variation will be reduced (Beria et al., 2018).

A second step is the assignment of a sampling date for rainfall and snowfall isotope samples, which are often composite (bulk) samples, collected over several precipitation events. The tested date assignment options are summarized in Table 1. For snowpack samples, the tested date assignments also include the date of the previous snowfall and the weighted average date of the entire accumulation period.

The third step is the integration of multiple spatial precipitation samples taken at the same date, either at different locations in the catchment, at a single location or elevation band but in the form of replicates or at different depths of a snowpack (Table 1). The combination of these options for weighting, date assignment and spatial integration lead to a total of 6720 possible methodological combinations for our datasets.

2.4 Estimation of F_{yw} with equivalent precipitation

Using P_{eq} as the input signal to the hydrological system, we have two options for F_{yw} estimation. The first is to simply replace the precipitation isotope signal, C_P with that of equivalent precipitation, C_{Peq}, assuming that C_{Peq} obtained from snowpack modelling can also be represented with by a sine curve with an amplitude, A_{Peq}. We will refer to this approach as the "snowpack modified amplitude ratio approach" and denote it as $F_{yw,Peq}=A_Q/A_{Peq.}$. The second option is based on the convolution approach with C_{Peq} as input signal, which we denote as $F_{yw,Conv.}$

To quantify the impact of using equivalent precipitation as the input isotopic signal rather than precipitation alone for F_{yw} estimation in snow dominated environments, we compare the results from the above two methods with F_{yw} estimates obtained from using A_P directly, denoted as $F_{yw,P} = A_Q/A_P$. We also compare the results to an even simpler snowpack-accounting method, which consists of directly weighting the precipitation isotope signal with the simulated amounts of equivalent precipitation (rather than first

simulating the isotope signal of equivalent precipitation). The corresponding isotope time-series is denoted C_{P*} and the estimated young water fraction is called $F_{yw,P*}$.

2.5 Parameter and uncertainty estimation

The fitting of sine curves to the times series of isotope values can be achieved with standard estimation tools. We use the default nonlinear least squares fitting algorithm implemented in the Matlab fit function, the trust region algorithm. Using the estimated mean and variance of the sine curve parameters obtained with this algorithm, we evaluate the standard deviation of $F_{yw,P}$, $F_{yw,P*}$ and $F_{yw,Peq}$ with Gaussian error propagation (similar to von Freyberg et al., 2018) as follows: we generate 10'000 random samples of the sine curve amplitudes (assuming they have a Gaussian distribution), build the corresponding amplitude ratios and then compute their standard deviations. Note that this method for error propagation assumes that the input and output amplitudes are independent, which is in reality not the case. This uncertainty estimation can thus be assumed to overestimate the variance.

For the optimal parameter identification in the convolution approach, we use the "fminsearch" function implemented in Matlab 2018b, which is a nonlinear programming solver that uses the simplex search method of Lagarias, Reeds, Wright, and Wright (1998), a direct search method without gradients. In addition, we use a Metropolis-Hastings algorithm (e.g. Kuczera & Parent, 1998) with additive Gaussian noise and uniform priors (implemented by Jbabdi, 2020) to produce samples from the posterior distribution of the Gamma parameters and thereby quantify the uncertainty of the convolution approach as a standard deviation.

In addition to the above parameter uncertainty ranges that result from the amplitude ratios or from the inference of Gamma parameters in the convolution approach, we also estimate the full range of uncertainty associated with the composition of the input isotope signal (Section 2.5), i.e. we compute the standard deviations resulting from 6720 combinations of weighting, date assignment and sample aggregation options, and compute the uncertainty around the sine wave parameter terms during the fitting process for both C_Q and C_P.

However, in order not to overestimate the total uncertainty range, we fix the precipitation isotope phase based on *a priori* physical knowledge. Specifically, as the variation in precipitation isotopes is largely driven by cloud condensation temperature (e.g. Beria et al., 2018; Puntsag et al., 2016), with colder temperatures resulting in more depleted isotopes, we set the phase of the sine wave so that the most depleted values of precipitation isotopes correspond to the same date as the minimum of the air temperature sine curve, since it dominates over possible factors influencing the variation in isotopic signature in precipitation.

All computations are completed in Matlab 2018b (Version 9.4), with the Statistics and Machine Learning Toolbox Version 11.3 and the Curve Fitting Toolbox Version 3.5.7.

3 Study catchments and datasets

We apply the above methods to three catchments in the Swiss and Italian Alps (Figure 1), which all experience snowmelt dominated streamflow regimes and a distinct low flow period during the winter snow accumulation period. However, all three catchments show a distinctive streamflow behavior during the snowmelt period (Figure 2) that is the result of a combination of different hydro-climatic factors (Tables 2 and 3).

3.1 Vallon de Nant (VdN)

VdN is a glacierized 13.4 km^2 catchment located in the Swiss Alps, with an elevation range between 1200 and 3051 m a.s.l. Table 2. The catchment is steep, with a mean slope of 36°, and the upper part houses the 0.36-km^2 Glacier des Martinets but is dominated by bare rocks and scree slopes. At mid elevations alpine grassland prevails (33% of *a*) to lower elevations, where it is mixed with forest which covers 16% of the catchment.

A network of four distributed meteorological stations (at 1253, 1530, 1780 and 2136 m a.s.l.) measured precipitation and air temperature with Lufft-WS 300/400 (Fellbach, Germany) instruments, and was used to determine the temperature lapse rate for VdN (Figure 1). Data from the Swiss automatic meteorological station network is used to gap fill the local observations (i.e., 12 missing days in 2017). A stream gauging station in the Avançon defines the catchment of the VdN (Figure 1). Streamflow was measured (VEGAPULS WL-61 optical height gauge, VEGA, Schiltach, Germany) over a geophone weir (installed by the Swiss Federal Institute for Forest, Snow and Landscape Research) and was determined by a rating curve (Ceperley et al., 2018).

Bulk rain samples were collected for isotopic analyses using funnels flowing into insulated bags at three locations corresponding to the rain gauges (1253, 1500, and 2100 m a.s.l.), and emptied weekly or biweekly between June 2016 and November 2018. Aggregation of these samples occurred according to various options presented subsequently. Between February 2016 and April 2018, snow samples were collected from the entire snow profile at various locations in the catchment (Figure 1, Table S1). Stream water at the VdN catchment outlet was sampled both manually and automatically by an ISCO sampler (Teledyne ISCO, USA, Table S1, Figure S1). Isotopic analyses of rain, snow and stream water were performed using a wavelength-scanned cavity ring down spectrometer (WS-CRDS 2140-I, Picarro, Santa Clara, California, USA).

For snowpack parameter estimation, SCA was calculated as a ratio from 0 to 1 over the non-forested part of the catchment using 21 Landsat 8 images, and 24 Sentinel 2 images retrieved between September 2016 and December 2017 (Michelon, Ceperley, Beria, Larsen, & Schaefli, 2018). A linear interpolation of the combined time-series was used to provide a fractional SCA per sampling date.

3.2 Noce Bianco at Pian Venezia (NBPV)

NBPV is a glacierized 8.4-km^2 catchment located in the Eastern Italian Alps (Table 2), with a long history of glaciological, hydrological and meteorological observations (Carturan, 2016; Carturan et al., 2013; Carturan et al., 2014; Carturan et al., 2016) with an elevation that ranges from 2298 to 3769 m a.s.l.. The upper part of NBPV is covered by the 3.5-km^2 La Mare Glacier, which sustains streamflow during the ablation season, while the lower part is mainly covered by bare rocks, discontinuous Alpine grassland and shrubs. Snow generally accumulates on the ground from October/November to April/May. Outside the glacier, snowmelt starts in May and can last until the end of June. Snowfalls can also occur during summer, as in 2014, but they tend to be rare at lower elevations. Based on the depth of the winter snowpack and the melting rates, ice melt can start in July (e.g., in 2015) or mid-August (Zuecco, Carturan, et al., 2019).

Daily air temperature and precipitation data were collected at a weather station (elevation: 2605 m a.s.l.), about 2 km away from the catchment (Figure 1). Streamflow was recorded by a water pressure recorder

(MDS Dipper-PTEC, SEBA Hydrometrie GmbH & Co, Kaufbeurenthe, Germany) at the outlet of the catchment (Table 2) at the hourly timescale (Carturan et al., 2016).

In this study, we considered the 2012-2015 period due to the availability of isotopic data for precipitation and stream water (Table S1, Figure S1). Bulk samples of rain were collected generally monthly from June to September at the outlet of NBPV (at 2298 m a.s.l.). Due to the difficult accessibility of NBPV during winter, snowpack samples collected at the end of the accumulation season (in May) at different elevations on and outside the glacier (Figure 1) were considered as a proxy of winter precipitation. Stream water samples were collected at the outlet of the catchment both manually and automatically by an ISCO sampler (Teledyne ISCO, USA) at the daily or subdaily timescale during summer (Zuecco, Carturan, et al., 2019). Samples isotopic composition was determined by off-axis integrated cavity output spectroscopy (OA-ICOS, DLT-100 model, Los Gatos Research Inc., USA).

SCA in the NBPV catchment was mapped manually using oblique terrestrial photographs and Landsat imagery (Zuecco, Carturan, et al., 2019). SCA maps (15) were obtained for the three ablation seasons of 2013, 2014 and 2015 using ArcMap 9.3 (Esri, USA). Based on these maps and the analysis of meteorological data, we estimated SCA for other periods, particularly to determine the duration of the accumulation season (Figure S2).

3.3 Bridge Creek Catchment (BCC)

BCC is a small catchment (0.14 km^2) located in the Eastern Italian Alps (Dolomites), with a long-term hydrological monitoring (Zuecco, Penna, & Borga, 2018). The high elevation (1932-2515 m a.s.l.) and the location in a sheltered part of the mountain range mean that streamflow is mainly sustained by snowmelt and summer storm events (Guastini et al., 2019; Zuecco et al., 2018). Land cover consists of Alpine grassland, and very few larch trees (Table 2). BCC lies on geological formations both from dolomite, *Dolomia Cassiana,* and carbonate and terrigenous clay and sandstone*, San Cassiano* (Penna, Zuecco, et al., 2017; Zuecco, Rinderer, Penna, Borga, & van Meerveld, 2019).

Precipitation and air temperature were measured by heated tipping buckets and temperature sensors at weather stations at 1645 and 2155 m a.s.l. (operated by the Agency for Environmental Protection of Veneto Region, ARPAV), about 2.5 km to the East and West of BCC. Precipitation data were interpolated using the inverse distance weighted method (Penna, Zuecco, et al., 2017). Stream levels were measured at a 15-min resolution by pressure transducers (Keller AG für Druckmesstechnik, Switzerland) installed behind a V-notch weir at the outlet of BCC (Figure 1) and were converted to streamflow based on the weir equation (Zuecco et al., 2018).

Bulk samples of rainwater were collected close to the outlet of BCC, approximately monthly from May to October 2011-2016 (Table S1, Figure S1). Additional rainwater samples were collected during selected rainfall events in summer 2010 and 2011 (Penna, van Meerveld, Zuecco, Fontana, & Borga, 2016). Snow cores collected during winter and early spring were considered representative of the isotopic composition of winter precipitation (Figure 1). Stream water samples were collected at the outlet manually during selected rainfall and snowmelt events, and approximately monthly from May to October 2011-2016. The isotopic composition of the samples was determined by OA-ICOS (DLT-100 model, Los Gatos Research Inc., USA).

In absence of SCA data, we determined the duration of the snow accumulation period according to the time-series of daily snow depth monitored by ARPAV at a station (elevation: 2227 m a.s.l.) 6 km away from BCC (Figure S2) and validating with field observations (not shown).

4 Results

We first present key results regarding the snowpack model parameterization (Section 4.1), before discussing in detail how options to construct C_P from sparce samples impact the C_{P-fit} parameters (Section 4.2). We then present the results of F_{yw} estimation based on the ratio (Section 4.3) and the convolution approaches (Section 4.4).

4.1 Snowpack parameterization and validation

The snowfall thresholds T_{crit1} and T_{crit2} from Equation (1) were previously determined experimentally for NBPV (Carturan et al., 2019); for the other two study sites, they are calibrated based on the available snow cover area (SCA) or snow cover duration observations (Table 3 and Figure S2), jointly with the degree-day factor ζ. The parameters are selected by manual calibration using the prior parameter ranges given in Table 3, i.e. by trial and error, judging visually for each parameter combination the agreement between observed and modelled SCA or snow cover duration.

Figure S2 shows that the chosen parameters (Table 3) result in a simulated SCA that is similar to the observations, with a coefficient of determination of 0.91 for NBPV and of 0.90 for VdN. In the case of BCC, 94.3% of the instances with snow presence/absence observations were correctly simulated. Given that relatively few observations were available for the calibration of the snow model, we tested the sensitivity of $F_{yw,Conv}$ to different sets of the snowpack parameters (Figure S3). This sensitivity analysis shows that the snow parameters have little effect on the $F_{yw,Conv}$ close to the chosen values. The resulting time-series of P_{eq} and an example of C_{Peq} are shown in Figure 2.

4.2 Estimating sine curves based on observed data

In stream water, A_Q based on $C_{Q\text{-}obs}$ ($\delta^{18}O$), ranged from 0.40 to 1.54‰ (Table 4), with corresponding adjusted R^2 of 0.84, 0.58 and 0.81 for VdN, NBPV and BCC (Figure 3, Table S2). The relatively low adjusted R^2 for NBPV is likely due to the temporal variability in $\delta^{18}O$ in the stream across the three summers (Figure 3). The mean isotopic values of stream water differ on average 9.5‰, 8.0‰, and -2.0‰ for VdN, NBPV, and BCC, from C_{P-fit} of 17.5% (VdN), 4.6% (NBPV) and -3.6 % (BCC) compared to P_{eq} (Table S3).

For precipitation, the full tested range of weighting, date assignment and sample aggregation options for rain and snow leads to a considerable variability in the C_{P-fit} (Figure 3), with the adjusted R^2 ranging from 0.27 to 0.88, from -0.23 to 0.90 and from 0.26 to 0.97 for VdN, NBPV and BCC, respectively. The worst fits for NPBV (with adjusted R^2 <0) are removed from further analysis. The resulting A_P range is 0.92–- 7.79‰ (VdN), 0.01–- 10.94‰ (NBPV) and 3.24–- 7.24‰ (BCC) and corresponding mean values of -11.6, -13, and -12.8‰ for VdN, NPBV and BCC, respectively (Tables 4 and S3).

Since the proposed snow isotope model takes as input the sine-fitted continuous precipitation isotope time-series C_P, the simulated C_{Peq} time-series also closely follows a sine curve (Figure 4). Accordingly, sine curves fitted to weighted C_{Peq} time-series have R^2 values close to 1 for all case studies, with median A_{Peq} of 5.19‰ for VdN, 2.33‰ for NBPV and 4.88‰ for BCC (Table 4). The reduction of A_{Peq} compared to A_P is only dramatic in the case of NBPV, where the ratio A_{Peq}/A_P is 0.52 for NBPV. For C_{P*}, the weighting of C_P

with equivalent precipitation amounts results in $A_{P*}>A_{P,}$ for 44% of all time-series methodology options in VdN, for 75% of all options in NBPV and for 74% in BCC. Median A_{P*} equals 4.32‰ (VdN), 7.56‰ (NBPV) and 5.4‰ (BCC).

The phase of isotopes in precipitation is forced to match the phase of air temperature, and results in median phases of 116, 122 and 119 days for VdN, NBPV and BCC (Table S4). Conversely, the phase of the sine curve of isotopes in stream water varies between 145 (BCC) to 179 (NBPV) to 245 days (VdN), corresponding to a phase difference between precipitation and streamflow ranging from 26 days (BCC) to 57 days (NBPV) and 129 days (VdN) (i.e., 1, 2, and 4 months). The weighting with P_{eq} has very little effect on the phase differences between C_{P*} and streamflow, which are on average very close to those for C_P, with 27 days (BCC), 70 days (NBPV) and 132 days (VdN). In comparison, the phase difference between sine curves fitted to C_{Peq} and to C_Q equals 11 days for BCC, 20 days for NBPV and 123 for VdN. Note that for C_{P*}, we weight the precipitation isotope time-series, and not the fitted precipitation sine curves with simulated equivalent precipitation amounts.

Inspecting the full distributions of A_P (across all methodological choices, Figure S4) shows that A_P is more sensitive to the date assignment of the bulk rainwater than to other methodological choices for rain samples. However, the methodological choices for handling snow sample impacts A_P far more than rain sample method choices. The choice of the date assignment for snow samples has a large impact on the estimated A_P for VdN and BCC. Conversely, A_P in the NBPV are more sensitive to the weighting options for snow samples and to the handling of multiple snow samples. The consequence of method choice for handling multiple rainwater samples is negligible for the estimated A_P in NBPV and BCC, due to the single sampling site per catchment, and only a few days with multiple samples.

4.3 Estimation of young water fractions using the amplitude ratio method

For VdN and BCC, applying the obtained A_P range (Table 4) to F_{yw} estimation results in relatively similar median values between $F_{yw,P}$ and $F_{yw,Peq}$ (Table 6, Figure 5) that are within 10%, yet the distributions are nevertheless significantly different (p<0.05, Wilcoxon rank sum test). For NBPV, the median $F_{yw,P}$ (33%) considerably underestimates the median $F_{yw,Peq}$ (63%). Furthermore, for NBPV, $F_{yw,P}$ and $F_{yw,Peq}$ show strongly bimodal distributions (Figure S5), with the modes centered at 20-40% for $F_{yw,P}$ and at 35-75% for $F_{yw,Peq.}$ We could not, however, clearly detect which mode is associated with a particular time-series construction option.

As shown in Figure S5, $F_{yw,Peq}$ has for all case studies much narrower distributions of standard deviations than $F_{yw,P}$. These standard deviations are related to the sine fit error, which is by construction relatively low for C_{Peq} since it is generated using the sine fit to C_P as an input (see Section 4.2). For all three case studies, the simplest possible approach using C_{P*} yields median $F_{yw,P*}$ values that are significantly different from those obtained for $F_{yw,Peq}$. In addition $F_{yw,P*}$ yields unrealistically high uncertainty ranges (Figure 5, left).

4.4 Estimation of young water fractions using the convolution method

The convolution approach uses C_{Peq} directly as an input signal and the sine fit to the C_Q as output signal. The resulting Gamma distribution parameters for the reduced range of time-series methodology options are summarized in Table 5 and Figure 6. The estimated mean $F_{yw,Conv}$ values and their distributions across all options (Table 6, Figure 5) are close to those from the amplitude ratio approach ($F_{yw,P,}$ $F_{yw,Peq,}$ $F_{yw,P*}$) for VdN and BCC, albeit with significantly higher median values, of 12% for VdN and BCC. For NBPV, the

distribution of $F_{yw,Conv}$ has a tail that spans up to 1, but the bimodality of $F_{yw,P,}$ is obscured by the full range of uncertainty. The mean value of 34% is higher than the value of $F_{yw,P}$ (33%), but considerably lower than $F_{yw,Peq}$ (63%).

$F_{yw,Conv}$ has a relatively narrow range of standard deviations (Figure 6). These standard deviations are related to the inferred posterior distributions of the Gamma parameters (α and β) per time-series option, i.e. the parameter distributions obtained through the parameter identification algorithm (the Metropolis-Hastings algorithm, see Section 2.5). The narrow range of these distributions of α and β highlights that the error associated with the identification of the best Gamma parameters is low (see Figure S6, Table S5). This low error is due to the fact that the input to the convolution, C_{Peq}, shows a shape that is close to a sine curve (Figure 4). Accordingly, the best Gamma distribution to reproduce the output sine curve is relatively well defined.

5 Discussion

5.1 Accounting for snow impacts on young water fraction estimation

Our results demonstrate that the simplest possible snow accounting method (weighting precipitation isotopes with equivalent precipitation amounts) can result in misleading F_{yw} estimates. In fact, comparing the distributions of $F_{yw,P*}$ with $F_{yw,Peq}$ and $F_{yw,Conv}$ (Figure 5) shows that although the median estimates from the three methods may be close, $F_{yw,P*}$ clearly yields far higher uncertainty ranges. The most striking example is the VdN case study, where we have the most samples (scenario of best data availability), but where the $F_{yw,P*}$ estimates are far more uncertain than the $F_{yw,Peq}$ or $F_{yw,Conv}$ estimates. Accordingly, we do not further discuss the use of the $F_{yw,P*}$ method.

The results show significant differences in the distributions of estimated F_{yw} values between the traditional methods that use total precipitation alone, and our estimates of F_{yw} that explicitly account for snow, even if the differences among median $F_{yw,P}$, $F_{yw,Peq}$ and $F_{yw,Conv}$ values are very small (in most cases, <1%). The difference between $F_{yw,P}$ and $F_{yw,Peq}$ should, however, not be interpreted as being due to snowpack processes directly, but rather as the bias generated through using total precipitation isotopes alone for F_{yw} estimation.

Inspecting the full range of F_{yw} distributions across all methods, an important distinction is evident with the amplitude ratio approach based on equivalent precipitation, i.e. $F_{yw,Peq}$, which can give significantly different estimates of the overall uncertainty compared to the convolution approach, especially in the case of NBPV. Here, the C_{Peq} shows a strong deviation from the sine wave fitted directly to precipitation (in terms of both shape and phase, Figure 4). This strong deviation of $F_{yw,Peq}$ estimates compared to $F_{yw,Conv}$ suggests that the convolution approach may be more appropriate for glacier and snow dominated Alpine catchments, where the delayed water input from melt may result in strongly non-sinusoidal input signals.

5.2 Sources of uncertainty in young water fraction estimation

Our results highlight the relatively large range of uncertainty on F_{yw} estimates that can arise from the construction of continuous isotope input time-series based on sparse samples, in particular for NBPV, which only has data during the melt season. For this case study, sine curve fitting to the observed P data is more uncertain than for the other case studies, resulting in a median standard deviation for $F_{yw,P}$ of 0.07 for NBPV, but only 0.01 for both VdN and BCC (Figure S5). More important, however, is the uncertainty arising from the different time-series fitting options, which results in a median value of standard deviations for $F_{yw,P}$ of 0.12 for NBPV (0.02 for VdN and 0.01 for BCC, Table 6).

The F_{yw} values are particularly sensitive to the treatment of snowpack samples; specifically, F_{yw} values are sensitive to how multiple spatial snow samples collected on the same day are aggregated, and how weights and dates are assigned to these snow samples (Figure S4). This sensitivity is a natural consequence of the high variability in the isotopic composition of snow samples across space (even at sampling sites few meters apart) and time (Beria et al., 2018; Schmieder et al., 2018; Zuecco, Carturan, et al., 2019). In an ideal scenario, if field conditions permitted year-round, exhaustive sampling, observations would be made at adequately high spatial and temporal resolutions.

What emerges from all three case studies is that the uncertainty on F_{yw} values (for $F_{yw,P}$, $F_{yw,Peq}$ and $F_{yw,Conv}$) generated by methodological choices in the construction of precipitation time-series is of the same order of magnitude as the uncertainty related to the sine curve fitting itself (~2%, Table 6). We do not provide a formal assessment of the full parameter uncertainties related to the snowpack simulation; however, our sensitivity analysis (Figure S2) shows that F_{yw} estimation is relatively insensitive to the snowpack parameters in the vicinity of the retained parameters.

Overall, the resulting uncertainty range for F_{yw} in VdN and BCC is relatively well constrained (<7%); however, in the glacier dominated catchment, NBPV, the uncertainty range increases substantially to 22%. This observation reveals that our approach to accounting for the impact of times series construction choices provides a useful framework for future F_{yw} studies in high elevation catchments, and demonstrates utility in obtaining robust F_{yw} estimates that can better identify the range of uncertainties with sub-optimal data availability and perhaps even help optimize sampling campaigns. However, such a F_{yw} estimation framework still crucially depends on the capability of the sampling effort to capture the entire variability in the streamflow isotopic signal; this effort, in the case of snow dominated catchments, requires intensive sampling throughout late winter and early spring, possibly at subweekly temporal resolution to improve the robustness of the F_{yw} estimates (Stockinger et al., 2016).

5.3 Comparison with existing young water fraction estimates from the European Alps

The three Alpine catchments tested as case studies have F_{yw} in the ranges of those previously observed in 22 Swiss catchments by von Freyberg et al. (2018, Figure 7), although our analysis is helpful in extending the elevation coverage. Similarly, our are consistent with the spread of F_{yw} (7-23%) for a catchment in the Canadian Rockies ranging in elevation from 1200 to 3500 m. a.s.l. (Campbell, Pavlovskii, & Ryan, 2020). von Freyberg et al. (2018) identified a relationship between F_{yw} and mean catchment elevation, to which two of our case studies (VdN and BCC) conform. Specifically, a decrease in catchment F_{yw} occurs above 1500 m a.s.l., a catchment elevation that has already been identified as corresponding to the transition between intermittent and seasonal snow cover (Beria, Larsen, Ceperley, Michelon, & Schaefli, 2019; Santos et al., 2018). However, given that our highest elevation study site (NBPV) deviates from this trend by yielding a higher F_{yw}, it is too early to draw the conclusion that low F_{yw} could be due to seasonal versus intermittent snow cover dynamics alone. The generally low F_{yw} values of these catchments at elevations higher than 1500 m a.s.l. are also consistent with the results by Jasechko et al. (2016), who found lower F_{yw} with increasing slope, and may be partially explained by higher subsurface storage in some higher elevation catchments (Staudinger et al., 2017). The relatively high F_{yw} obtained for the higher elevation glacier dominated catchment highlights that much more research from these systems is needed to derive a process-based explanation for F_{yw} in Alpine catchments, though lower storage and faster drainage from glacier systems have been argued in the past (Jansson, Hock, & Schneider, 2003). In addition, better seasonal sampling coverage could reduce the uncertainty range and improve F_{yw} estimation.

6 Conclusion

This study proposes a readily reproducible framework to estimate fractions of young water (F_{yw}) from the dampening of observed stable isotope variations between precipitation and streamflow in snow dominated catchments, i.e. in catchments with a seasonal snow cover that leads to a strong shift in the input of winter precipitation to spring and summer streamflow. The framework includes a parsimonious snow model that is tested for three study catchments selected from the Swiss and Italian Alps and provides a distribution of F_{yw} values that incorporates all possible methodological choices and uncertainties. This workflow demonstrates the extreme sensitivity of snow dominated catchments to the input time-series of isotope composition, which arises from both the variability of observations (of rain and snow) as well as the sequence of methods used to combine them into continuous input time-series. Despite including a simple snow model to account for delays in hydrological inputs, without sufficiently high temporal (or spatial) resolution of isotopic observations, the uncertainties propagated by interpolation choices dominate the overall uncertainty of the F_{yw}.

In addition, we find that the commonly used amplitude ratio approach can bias the results in snow dominated catchments, in particular for cases with sparse sample availability or when equivalent precipitation inputs are strongly non-sinusoidal. Instead, we propose that our approach of inverse estimation of F_{yw} via convolution might be better suited for these situations. The estimated F_{yw} values for the three case studies are broadly in agreement with previous findings in the Swiss Alps. High elevation catchments can have very low F_{yw}, which cannot be explained by snow storage alone, and are likely the product of higher subsurface storage and associated drainage processes, with the exception of very high glacier dominated catchments. Our results demonstrate that the F_{yw} estimation technique can be extended to account for a range of uncertainties and hydrological pathways and stresses the need for further work on F_{yw} in snow and glacier dominated catchments.

Author contributions

The paper was written by NC, GZ and BS with contributions from all co-authors. NC, JRL, BS and GZ designed the study. NC, GZ, BS, HB, and LC made substantial contributions to the analysis and interpretation of the data. Data related to VdN were collected and archived by AM and NC. Data related to NBPV and BCC were collected and archived by GZ, LC, and DP. AM provided critical feedback during the data analysis and writing phase of this study. All authors revised the manuscript and gave final approval to the submitted version.

Acknowledgements

The work of HB, NC, AM and BS was funded by the Swiss National Science Foundation (SNSF), grant number PP00P2_157611. GZ acknowledges the financial support provided by Fondazione Cassa di Risparmio di Padova e Rovigo (Italy) (research project "Ecohydrological Dynamics and Water Pathways in Forested Catchments", Bando Starting Grants 2015) and DOR2019 (research project "Analisi dei processi di generazione di deflusso in bacini d'alta quota", University of Padova, Italy). We thank Marco Borga for providing comments on an earlier version of the manuscript.

Data Availability

The data that support the findings of this study are available from the corresponding author upon reasonable request.

606

References

Ala-Aho, P., Tetzlaff, D., McNamara, J. P., Laudon, H., Kormos, P., & Soulsby, C. (2017). Modeling the isotopic evolution of snowpack and snowmelt: Testing a spatially distributed parsimonious approach. *Water Resources Research, 53*(7), 5813-5830. doi:10.1002/2017WR020650

Ala-aho, P., Tetzlaff, D., McNamara, J. P., Laudon, H., & Soulsby, C. (2017). Using isotopes to constrain water flux and age estimates in snow-influenced catchments using the STARR (Spatially distributed Tracer-Aided Rainfall-Runoff) model. *Hydrology and Earth System Sciences, 21*(10), 5089-5110. doi:10.5194/hess-21-5089-2017

Amin, I. E., & Campana, M. E. (1996). A general lumped parameter model for the interpretation of tracer data and transit time calculation in hydrologic systems. *Journal of Hydrology, 179*(1-4), 1-21. doi:10.1016/0022-1694(95)02880-3

Benettin, P., Soulsby, C., Birkel, C., Tetzlaff, D., Botter, G., & Rinaldo, A. (2017). Using SAS functions and high-resolution isotope data to unravel travel time distributions in headwater catchments. *Water Resources Research, 53*(3), 1864-1878. doi:10.1002/2016wr020117

Beria, H., Larsen, J. R., Ceperley, N. C., Michelon, A., & Schaefli, B. (2019). *Increased occurrence of ephemeral snowpacks will augment groundwater recharge and worsen summer low flow conditions in the Alps.* Paper presented at the AGU Fall Meeting, San Francisco, CA, USA.

Beria, H., Larsen, J. R., Ceperley, N. C., Michelon, A., Vennemann, T., & Schaefli, B. (2018). Understanding snow hydrological processes through the lens of stable water isotopes. *Wiley Interdisciplinary Reviews-Water, 5*(6), null. doi:10.1002/wat2.1311

Beria, H., Larsen, J. R., Michelon, A., Ceperley, N. C., & Schaefli, B. (2020). HydroMix v1.0: a new Bayesian mixing framework for attributing uncertain hydrological sources. *Geoscientific Model Development, 13*(5), 2433-2450. doi:10.5194/gmd-13-2433-2020

Birkel, C., Soulsby, C., & Tetzlaff, D. (2015). Conceptual modelling to assess how the interplay of hydrological connectivity, catchment storage and tracer dynamics controls nonstationary water age estimates. *Hydrological Processes, 29*(13), 2956-2969. doi:10.1002/hyp.10414

Campbell, É. M. S., Pavlovskii, I., & Ryan, M. C. (2020). Snowpack disrupts relationship between Fyw and isotope amplitude ratio; approximately 1/5 of mountain streamflow less than one year old. *Hydrological Processes, n/a*(n/a). doi:10.1002/hyp.13914

Carturan, L. (2016). Replacing monitored glaciers undergoing extinction: a new measurement series on La Mare Glacier (Ortles-Cevedale, Italy). *Journal of Glaciology, 62*(236), 1093-1103. doi:10.1017/jog.2016.107

Carturan, L., Baroni, C., Becker, M., Bellin, A., Cainelli, O., Carton, A., . . . Seppi, R. (2013). Decay of a long-term monitored glacier: Careser Glacier (Ortles-Cevedale, European Alps). *The Cryosphere, 7*(6), 1819-1838. doi:10.5194/tc-7-1819-2013

Carturan, L., Baroni, C., Carton, A., Cazorzi, F., Dalla Fontana, G., Delpero, C., . . . Zanoner, T. (2014). Reconstructing Fluctuations of La Mare Glacier (Eastern Italian Alps) in the Late Holocene: New Evidence for a Little Ice Age Maximum Around 1600 AD. *Geografiska Annaler Series a-Physical Geography, 96*(3), 287-306. doi:10.1111/geoa.12048

Carturan, L., De Blasi, F., Cazorzi, F., Zoccatelli, D., Bonato, P., Borga, M., & Dalla Fontana, G. (2019). Relevance and Scale Dependence of Hydrological Changes in Glacierized Catchments: Insights from Historical Data Series in the Eastern Italian Alps. *Water, 11*(1), 25. doi:10.3390/w11010089

Carturan, L., Zuecco, G., Seppi, R., Zanoner, T., Borga, M., Carton, A., & Dalla Fontana, G. (2016). Catchment-Scale Permafrost Mapping using Spring Water Characteristics. *Permafrost and Periglacial Processes, 27*(3), 253-270. doi:10.1002/ppp.1875

Ceperley, N., Michelon, A., Escoffier, N., Mayoraz, G., Boix Canadell, M., Horgby, A., . . . Boss, S. (2018). Salt Gauging And Stage-Discharge Curve, Avançon De Nant, Outlet Vallon De Nant Catchment. In: Zenodo.

Dahlke, H. E., Lyon, S. W., Jansson, P., Karlin, T., & Rosqvist, G. (2014). Isotopic investigation of runoff generation in a glacierized catchment in northern Sweden. *Hydrological Processes, 28*(3), 1383-1398. doi:10.1002/hyp.9668

Douinot, A., Tetzlaff, D., Maneta, M., Kuppel, S., Schulte-Bisping, H., & Soulsby, C. (2019). Ecohydrological modelling with EcH2O-iso to quantify forest and grassland effects on water partitioning and flux ages. *Hydrological Processes, 33*(16), 2174-2191. doi:10.1002/hyp.13480

Engel, M., Penna, D., Bertoldi, G., Dell'Agnese, A., Soulsby, C., & Comiti, F. (2016). Identifying run-off contributions during melt-induced run-off events in a glacierized alpine catchment. *Hydrological Processes, 30*(3), 343-364. doi:10.1002/hyp.10577

Fang, Z. F., Carroll, R. W. H., Schumer, R., Harman, C., Wilusz, D., & Williams, K. H. (2019). Streamflow partitioning and transit time distribution in snow-dominated basins as a function of climate. *Journal of Hydrology, 570*, 726-738. doi:10.1016/j.jhydrol.2019.01.029

Guastini, E., Zuecco, G., Errico, A., Castelli, G., Bresci, E., Preti, F., & Penna, D. (2019). How does streamflow response vary with spatial scale? Analysis of controls in three nested Alpine catchments. *Journal of Hydrology, 570*, 705-718. doi:10.1016/j.jhydrol.2019.01.022

Harpold, A. A., Kaplan, M. L., Klos, P. Z., Link, T., McNamara, J. P., Rajagopal, S., . . . Steele, C. M. (2017). Rain or snow: hydrologic processes, observations, prediction, and research needs. *Hydrology and Earth System Sciences, 21*(1), 1-22. doi:10.5194/hess-21-1-2017

He, Z. H., Parajka, J., Tian, F. Q., & Bloschl, G. (2014). Estimating degree-day factors from MODIS for snowmelt runoff modeling. *Hydrology and Earth System Sciences, 18*(12), 4773-4789. doi:10.5194/hess-18-4773-2014

Hock, R. (2003). Temperature index melt modelling in mountain areas. *Journal of Hydrology, 282*(1-4), 104-115. doi:10.1016/S0022-1694(03)00257-9

Hrachowitz, M., Benettin, P., van Breukelen, B. M., Fovet, O., Howden, N. J. K., Ruiz, L., . . . Wade, A. J. (2016). Transit times-the link between hydrology and water quality at the catchment scale. *Wiley Interdisciplinary Reviews: Water, 3*(5), 629-657. doi:10.1002/wat2.1155

Huss, M., Bookhagen, B., Huggel, C., Jacobsen, D., Bradley, R. S., Clague, J. J., . . . Winder, M. (2017). Toward mountains without permanent snow and ice. *Earths Future, 5*(5), 418-435. doi:10.1002/2016ef000514

Jansson, P., Hock, R., & Schneider, T. (2003). The concept of glacier storage: a review. *Journal of Hydrology, 282*(1-4), 116-129. doi:10.1016/S0022-1694(03)00258-0

Jasechko, S., Kirchner, J. W., Welker, J. M., & McDonnell, J. J. (2016). Substantial proportion of global streamflow less than three months old. *Nature Geoscience, 9*(2), 126-+. doi:10.1038/Ngeo2636

Jbabdi, S. (2020). Metropolis Hastings. Retrieved from https://www.mathworks.com/matlabcentral/fileexchange/41231-metropolis-hastings

Kirchner, J. W. (2016a). Aggregation in environmental systems - Part 2: Catchment mean transit times and young water fractions under hydrologic nonstationarity. *Hydrology and Earth System Sciences, 20*(1), 299-328. doi:10.5194/hess-20-299-2016

Kirchner, J. W. (2016b). Aggregation in environmental systems – Part 1: Seasonal tracer cycles quantify young water fractions, but not mean transit times, in spatially heterogeneous catchments. *Hydrology and Earth System Sciences, 20*(1), 279-297. doi:10.5194/hess-20-279-2016

Kirchner, J. W. (2019). Quantifying new water fractions and transit time distributions using ensemble hydrograph separation: theory and benchmark tests. *Hydrology and Earth System Sciences, 23*(1), 303-349. doi:10.5194/hess-23-303-2019

Kuczera, G., & Parent, E. (1998). Monte Carlo assessment of parameter uncertainty in conceptual catchment models: the Metropolis algorithm. *Journal of Hydrology, 211*(1-4), 69-85. doi:10.1016/S0022-1694(98)00198-X

Lagarias, J. C., Reeds, J. A., Wright, M. H., & Wright, P. E. (1998). Convergence properties of the Nelder-Mead simplex method in low dimensions. *SIAM Journal on optimization, 9*(1), 112-147. doi:10.1137/S1052623496303470

Małoszewski, P., & Zuber, A. (1982). Determining the turnover time of groundwater systems with the aid of environmental tracers. *Journal of Hydrology, 57*(3-4), 207-231. doi:10.1016/0022-1694(82)90147-0

McGuire, K. J., & McDonnell, J. J. (2006). A review and evaluation of catchment transit time modeling. *Journal of Hydrology, 330*(3-4), 543-563. doi:10.1016/j.jhydrol.2006.04.020

Michelon, A., Ceperley, N., Beria, H., Larsen, J., & Schaefli, B. (2018, 2018). *Quantification of snowmelt processes in a high Alpine catchment from hydrographs, satellite images and stable water isotopes.* Paper presented at the EGU General Assembly.

Ohlanders, N., Rodriguez, M., & McPhee, J. (2013). Stable water isotope variation in a Central Andean watershed dominated by glacier and snowmelt. *Hydrology and Earth System Sciences, 17*(3), 1035-1050. doi:10.5194/hess-17-1035-2013

Ohmura, A. (2001). Physical basis for the temperature-based melt-index method. *Journal of Applied Meteorology, 40*(4), 753-761. doi:10.1175/1520-0450(2001)040<0753:Pbfttb>2.0.Co;2

Penna, D., Engel, M., Bertoldi, G., & Comiti, F. (2017). Towards a tracer-based conceptualization of meltwater dynamics and streamflow response in a glacierized catchment. *Hydrology and Earth System Sciences, 21*(1), 23-41. doi:10.5194/hess-21-23-2017

Penna, D., Engel, M., Mao, L., Dell'Agnese, A., Bertoldi, G., & Comiti, F. (2014). Tracer-based analysis of spatial and temporal variations of water sources in a glacierized catchment. *Hydrology and Earth System Sciences, 18*(12), 5271-5288. doi:10.5194/hess-18-5271-2014

Penna, D., van Meerveld, H. J., Zuecco, G., Fontana, G. D., & Borga, M. (2016). Hydrological response of an Alpine catchment to rainfall and snowmelt events. *Journal of Hydrology, 537*, 382-397. doi:10.1016/j.jhydrol.2016.03.040

Penna, D., Zuecco, G., Crema, S., Trevisani, S., Cavalli, M., Pianezzola, L., . . . Borga, M. (2017). Response time and water origin in a steep nested catchment in the Italian Dolomites. *Hydrological Processes, 31*(4), 768-782. doi:10.1002/hyp.11050

Pepin, N., Bradley, R. S., Diaz, H. F., Baraer, M., Caceres, E. B., Forsythe, N., . . . Grp, M. R. I. E. W. (2015). Elevation-dependent warming in mountain regions of the world. *Nature Climate Change, 5*(5), 424-430. doi:10.1038/Nclimate2563

Piovano, T. I., Tetzlaff, D., Ala-aho, P., Buttle, J., Mitchell, C. P. J., & Soulsby, C. (2018). Testing a spatially distributed tracer-aided runoff model in a snow-influenced catchment: Effects of multicriteria calibration on streamwater ages. *Hydrological Processes, 32*(20), 3089-3107. doi:10.1002/hyp.13238

Puntsag, T., Mitchell, M. J., Campbell, J. L., Klein, E. S., Likens, G. E., & Welker, J. M. (2016). Arctic Vortex changes alter the sources and isotopic values of precipitation in northeastern US. *Scientific Reports, 6*, 22647. doi:10.1038/srep22647

Rango, A., & Martinec, J. (1995). Revisiting the Degree-Day Method for Snowmelt Computations. *Water Resources Bulletin, 31*(4), 657-669. doi:10.1111/j.1752-1688.1995.tb03392.x

Rinaldo, A., Benettin, P., Harman, C. J., Hrachowitz, M., McGuire, K. J., van der Velde, Y., . . . Botter, G. (2015). Storage selection functions: A coherent framework for quantifying how catchments store and release water and solutes. *Water Resources Research, 51*(6), 4840-4847. doi:10.1002/2015wr017273

Rücker, A., Boss, S., Kirchner, J. W., & von Freyberg, J. (2019). Monitoring snowpack outflow volumes and their isotopic composition to better understand streamflow generation during rain-on-snow events. *Hydrol. Earth Syst. Sci. Discuss., 2019*, 1-37. doi:10.5194/hess-2019-11

Santos, A. C., Portela, M. M., Rinaldo, A., & Schaefli, B. (2018). Analytical flow duration curves for summer streamflow in Switzerland. *Hydrology and Earth System Sciences, 22*(4), 2377-2389. doi:10.5194/hess-22-2377-2018

Schaefli, B., Hingray, B., Niggli, M., & Musy, A. (2005). A conceptual glacio-hydrological model for high mountainous catchments. *Hydrology and Earth System Sciences, 9*, 95 - 109. doi:10.5194/hessd-2-73-2005

Schaefli, B., Nicotina, L., Imfeld, C., Da Ronco, P., Bertuzzo, E., & Rinaldo, A. (2014). SEHR-ECHO v1.0: a Spatially Explicit Hydrologic Response model for ecohydrologic applications. *Geoscientific Model Development, 7*(6), 2733-2746. doi:10.5194/gmd-7-2733-2014

Schmieder, J., Garvelmann, J., Marke, T., & Strasser, U. (2018). Spatio-temporal tracer variability in the glacier melt end-member - How does it affect hydrograph separation results? *Hydrological Processes, 32*(12), 1828-1843. doi:10.1002/hyp.11628

Smith, A., Tetzlaff, D., Laudon, H., Maneta, M., & Soulsby, C. (2019). Assessing the influence of soil freeze-thaw cycles on catchment water storage-flux-age interactions using a tracer-aided ecohydrological model. *Hydrology and Earth System Sciences, 23*(8), 3319-3334. doi:10.5194/hess-23-3319-2019

Sprenger, M., Leistert, H., Gimbel, K., & Weiler, M. (2016). Illuminating hydrological processes at the soil-vegetation-atmosphere interface with water stable isotopes. *Reviews of Geophysics, 54*(3), 674-704. doi:10.1002/2015rg000515

Sprenger, M., Tetzlaff, D., Buttle, J., Laudon, H., & Soulsby, C. (2018). Water ages in the critical zone of long-term experimental sites in northern latitudes. *Hydrology and Earth System Sciences, 22*(7), 3965-3981. doi:10.5194/hess-22-3965-2018

Staudinger, M., Stoelzle, M., Seeger, S., Seibert, J., Weiler, M., & Stahl, K. (2017). Catchment water storage variation with elevation. *Hydrological Processes, 31*(11), 2000-2015. doi:10.1002/hyp.11158

Stockinger, M. P., Bogena, H. R., Lucke, A., Diekkruger, B., Cornelissen, T., & Vereecken, H. (2016). Tracer sampling frequency influences estimates of young water fraction and streamwater transit time distribution. *Journal of Hydrology, 541*, 952-964. doi:10.1016/j.jhydrol.2016.08.007

Strasser, U., Bernhardt, M., Weber, M., Liston, G. E., & Mauser, W. (2008). Is snow sublimation important in the alpine water balance? *The Cryosphere, 2*(1), 53-66. doi:10.5194/tc-2-53-2008

Viviroli, D., Durr, H. H., Messerli, B., Meybeck, M., & Weingartner, R. (2007). Mountains of the world, water towers for humanity: Typology, mapping, and global significance. *Water Resources Research, 43*(7). doi:10.1029/2006wr005653

von Freyberg, J., Allen, S. T., Seeger, S., Weiler, M., & Kirchner, J. W. (2018). Sensitivity of young water fractions to hydro-climatic forcing and landscape properties across 22 Swiss catchments. *Hydrology and Earth System Sciences, 22*(7), 3841-3861. doi:10.5194/hess-22-3841-2018

Walck, C. (2007). Handbook on statistical distributions for experimentalists, Particle Physics Group, University of Stockholm, Stockholm. 202 pp.

Zuecco, G., Carturan, L., De Blasi, F., Seppi, R., Zanoner, T., Penna, D., . . . Dalla Fontana, G. (2019). Understanding hydrological processes in glacierized catchments: Evidence and implications of highly variable isotopic and electrical conductivity data. *Hydrological Processes, 33*(5), 816-832. doi:10.1002/hyp.13366

Zuecco, G., Penna, D., & Borga, M. (2018). Runoff Generation in Mountain Catchments: Long-Term Hydrological Monitoring in the Rio Vauz Catchment, Italy. *Cuadernos De Investigacion Geografica, 44*(2), 397-428. doi:10.18172/cig.3327

Zuecco, G., Rinderer, M., Penna, D., Borga, M., & van Meerveld, H. J. (2019). Quantification of subsurface hydrologic connectivity in four headwater catchments using graph theory. *Science of The Total Environment, 646*, 1265-1280. doi:10.1016/j.scitotenv.2018.07.269

Tables

Table 1: Tested options for the aggregation of isotopic data in precipitation and the related construction of sample time-series based on irregular samples (left columns for rain, right for snow). Each option is numbered; a complete set of methods is obtained by picking one choice per column (e.g. 122142).

Rain			Snow		
Assignment of date	**Weight selection**	**Multiple sampling handling**	**Assignment of date**	**Weight selection**	**Multiple sampling handling**
1: Day of collection	1: Depth (mm) in field	1: All rain samples	1: Collection day	1: Depth (mm) snow	1: All snow and snowpack samples, as individuals without averaging
2: Day of start of collection	2: Sum of all intermediary rain	2: Averaged by day	2: Start of snowpack date	2: Depth top layer	2: One composite per day per elevation
3: Midpoint of collection period		3: Average by day, weighted by rainfall collection volume	3: Midpoint of snowpack to collection	3: Depth of previous snowfall	3: Averaged by day
4: Day of intermediary peak precipitation		4: Only use single point	4: Date of peak snowfall since start of accumulation	4: Snowfall of whole accumulation period until collection	4: Snowpack average by day, weighted by depth
5: Weighted average of day			5: Date of previous snowfall		5: One snowfall per day per elevation
			6: Weighted average over whole accumulation period		6: Snowfall averaged by day
					7: Snowfall averaged by day weighted by snowfall depth

Table 2: Main characteristics of the three study catchments; Vallon the Nant (VdN) in the Swiss Alps, Noce Bianco at Pian Venezia (NBPV) and Bridge Creek Catchment (BCC) in the Italian Alps.

	VdN	NBPV	BCC
Outlet elevation (m a.s.l.)	1189	2298	1932
Mean elevation (m a.s.l.)	1966	3049	2121
Max elevation (m a.s.l.)	3051	3769	2515
Weather station elevation (m. a.s.l.)	1253	2605	1983
Length of the main stream (m)	5085	2738	277
Avg slope (°)	36	26	30
Area (km²)	13.5	8.4	0.14
Latitude	46.25	46.43	46.49
Longitude	7.11	10.67	11.84
Glacier cover (%)	3	42	0
Alpine grassland incl. bushes and pasture (%)	33	6	93
Rocks (bare rocks and scree slopes) (%)	47	52	7
Forest (%)	16	0	0
Open water (%)	1	0	0

Table 3: Main hydro-climatic characteristics of the three study catchments. Observation period is October 1, 2015 – January 1, 2019 for Vallon de Nant (VdN), October 1, 2011 – September 30, 2015 for Noce Bianco at Pian Venezia (NBPV), and October 1, 2009 – November 30, 2016 for Bridge Creek Catchment (BCC). Elevation of the reference weather station is 1253, 2605 and 1983 m a.s.l. for VdN, NBPV and BCC, respectively. Date of snowpack simulation start (initial SWE is set to zero on this date), selected snowpack parameters, and corresponding prior parameter ranges are also reported.

Hydrometeorological characteristic	**Period (average)**	**Prior parameter range**	**Study catchments**		
			VdN	**NBPV**	**BCC**
Air temperature (°C)	Annual	-	5.9	0.2	2.4
	Winter	-	2.9	-3.4	-1.0
	Summer	-	11.9	7.2	9.5
Precipitation (mm/yr)	Annual	-	1591	1413	1203
	Winter	-	977	978	656
	Summer	-	614	435	547
Streamflow (mm/day)	Annual	-	4.3	7.1	4.2
	Winter	-	3.1	1.4	4.2
	Summer	-	5.8	11.7	4.2
Baseflow (mm/day)	Annual	-	2.9	4.2	3.6
	Winter	-	2.1	1.2	3.6
	Summer	-	4.2	8.4	3.4
Temperature lapse rate (°C/km)	Annual	-	-3.7	-6.8	-5.7
Simulation start	-	-	01-Oct-2015	01-Oct-2011	01-Oct-2009
Minimum threshold of snowfall (T_{crit1}, °C)	Annual	[-1.0 - 0.0]	1.0	1.2	1.0
Maximum threshold of snowfall (T_{crit2}, °C)	Annual	[1.5 - 3.0]	3.0	3.2	3.0
Degree day factor (ζ, mm/°C/day)	Annual	[2.0 – 6.0]	3.5	5.0	2.7

Table 4: Estimated streamflow isotope amplitudes (A_Q, all weighted by Q, all values of $\delta^{18}O$ in ‰) and estimated ranges of sine curve amplitudes for precipitation isotopes, *P*, equivalent precipitation isotopes P_{eq} using all time-series construction options except assigning the snow date stamp to the date of collection (resulting in 5600 options). For NBPV, we also removed the 94 options for which $R^2<0$ for the sine fit to precipitation. For VdN, 16 of the remaining options lead *P** to a strong weighting of a few samples and an ensuing high amplitude (57.84) and upward shift of the entire sine curve (see mean sine curve values in Table S3, resulting in unrealistically high maximum values). 'Std' indicates the standard deviation of all mean values obtained per time-series construction option.

	VdN				NBPV				BCC			
	min	max	median	std	min	max	median	std	min	max	median	std
Q			0.40				1.54				0.49	
P	0.92	7.79	4.79	0.88	0.01	10.94	4.50	2.20	3.24	7.24	4.72	0.66
P_{eq}	1.00	8.44	5.19	0.95	0.01	5.67	2.33	1.14	3.35	7.48	4.88	0.68
P^*	0.47	57.88	4.32	3.21	0.97	24.69	7.56	3.82	1.81	18.20	5.40	2.11

Table 5: Range of Gamma parameters obtained with the full range of options to construct precipitation isotope time-series, except assigning the snow date stamp to the date of collection (resulting in 5600 options). 'Std' indicates the standard deviation of all mean values obtained per time-series construction option.

	VdN				NBPV				BCC			
	min	max	median	std	min	max	median	std	min	max	median	std
α	1.1	2.3	1.2	0.0	0.6	4.8	0.7	0.2	0.2	0.2	0.2	0.0
β	55	876	492	108	10	1291	286	163	191	3019	540	1310
τ	128	1005	594	118	50	712	194	86	39	644	109	282

Table 6: Range of young water fractions (F_{yw}) obtained with the different methods for the full range of options to construct precipitation isotope time-series, except assigning the snow date stamp to the date of collection (resulting in 5600 options). For the amplitude ratio approach, we also removed the 325 options for NBPV for which $R^2<0$ for the sine fit to precipitation and the 120 options where the *P** amplitude was greater than the Q amplitude. 'Std' indicates the standard deviation of all mean values obtained per time-series construction option. The final column by site shows the mean of standard deviations per method.

	VdN					NBPV					BCC				
	min	max	median	std	mean of std	min	max	median	std	mean of std	min	max	median	std	mean of std
$F_{yw,P}$	0.05	0.44	0.08	0.02	0.02	0.14	0.85	0.33	0.12	17.25	0.07	0.15	0.10	0.01	0.02
$F_{yw,Peq}$	0.05	0.40	0.08	0.02	0.00	0.27	1.63	0.63	0.23	0.04	0.07	0.15	0.10	0.01	0.01
$F_{yw,P*}$	0.01	0.84	0.09	0.07	1.51	0.06	1.58	0.21	0.22	9.97	0.03	0.27	0.09	0.03	0.01
$F_{yw,Conv}$	0.04	2.06	0.08	0.03	0.00	0.18	8.62	0.34	0.16	0.00	0.06	4.00	0.11	0.07	0.00

Figures

Figure 1: Location of the study catchments in Switzerland and Italy and position of weather stations and the main sampling sites for rainwater, snowpack and stream water. The catchment outlines are shown in black over aerial images, with indication of contour lines.

Figure 2: Daily precipitation (second left axis, black), daily mean air temperature (left axis, red), and hourly streamflow (right axis, blue) for the three study catchments in left column. Modeled snow water equivalent shown as mean snow depth, hs (left axis, blue), and snowmelt, M (right axis, cyan) in right column. Note that the scales of the dates and y-axes vary by catchment and variable.

Figure 3: Sine curve fitted to streamflow, Q, and variation in sine wave fitting to precipitation, P, isotopes, for all catchments. Grey scale shows adjusted R^2 for each possible C_P isotope fit. The best fit is highlighted in red; the circles show the used samples for that fit, sized relative to the weight. The best fit corresponds to options 312131 for VdN (R^2=0.88), 121444 for NBPV (R^2=0.90), 115131 for BCC (R^2=0.97) from Table 1. The date of minimum $\delta^{18}O$ in C_Q and C_P (forced by the air temperature) are shown as dashed vertical lines.

Figure 4: Example of convolution result. Input C_{Peq} isotopes (solid purple line) and isotopes in the output of the convolution ($C_{Q\text{-}Conv}$, solid cyan line), compared with the observations of isotopes in Q ($C_{Q\text{-}Obs}$, blue dots), corrected to the input mean, and the original sine wave of isotopes in P (C_P, dashed red line). The inferred Gamma distribution parameters α and τ for each site are shown. The selected C_P shown here is the same as in Figure 3.

Figure 5: Left column shows the distribution of mean F_{yw} over all time-series construction options for the reduced option range (5600 options, see Table 5) for the three catchments (a, c, e). Right column (b, d, f) shows the distribution of standard deviations around F_{yw} values resulting from Gaussian error propagation corresponding to the time-series construction options and catchments as in left column. F_{yw} values computed with the convolution approach (Conv, right most boxes) show standard deviations estimated from the posterior distributions of the Gamma parameters α and β.

Figure 6: Distribution of median Gamma parameters per time-series construction option for the reduced option range (5600 options, see Table 5). Left column shows α and right column β, and rows show the three sites, VdN, NBPV, and BCC.

Figure 7: Relation between F_{yw} and mean elevation for 22 Swiss catchments (grey circles sites < 1500 m. a.s.l. and black diamonds sites >1500 m. a.s.l., von Freyberg et al., 2018) and our three sites. Colored squares are F_{yw} from the theoretical amplitude dampening (application of eq. 8 of Kirchner, 2016a) with the inferred Gamma distribution, with error bars showing the standard deviation.

Figure Legends for Supporting Information

Figure S1. Flow duration curves for each study catchment. Isotope concentrations of individual samples are plotted according to the exceedance probability of the streamflow at the moment they were sampled.

Figure S2. Snowpack validation in two sites (VdN and NBPV) based on snow covered area (SCA) extracted from satellite data (solid black line with circles). The snowpack simulation in the third site (BCC) was done with snow depth measurements but only differentiated whether there was snow or not.

Figure S3. Subplots showing effect of snowpack parameters on the young water fraction ($F_{yw,Conv}$). In all subplots, the x-axis shows the degree day factor (ζ). The first row shows the effect of varying the minimum critical temperature (T_{crit1}), above which precipitation no longer falls exclusively as snow, the second row shows the effect of varying the maximum critical temperature (T_{crit2}), above which precipitation always falls as rain. The color axis shows the $F_{yw,\ Conv.}$ The columns are the different sites. The black circles show the parameters selected with the snowpack validation.

Figure S4. Boxplots showing the effect of choices (colors) for construction of time-series of precipitation on final $F_{yw,Conv}$ determined according to 4 methods (rows) at 3 sites (columns). Final row shows the adjusted R^2. Numbers (along x-axes) and names (legend) correspond to Table 1. In each box, the central dot indicates the median, edges of the solid box indicate the range of the 25th to 75th percentiles, whiskers extend to the most extreme data points and outliers are shown as open circles.

Figure S5: For each case study, the left (blue) plot shows the distribution of the mean and the right (orange) plot, shows the distribution of the standard deviation. The full range of values for all samples can be seen in the separate file, 'TableS5.xls'. The standard deviation shows the standard deviation per option, not the standard deviation across the options.

Figure S6: Distribution of standard deviations of Gamma parameters in the convolution approach (*Fyw,Conv*); shown is the distribution of tau (τ) and not β=τ/α since we inferred τ and not beta in the Matlab implementation.

Additional Files as part of Supporting Information

Additional File 1. 'Supportinginformation....doc' contains sections of the supporting information S1, Additional details regarding study catchments and data sets including Table S1, Sample count according to catchment, S2 Additional details regarding the Snowpack simulation, S3 Details on fitted sine curve parameters, including Tables S2, S3, S4, section S4 which contains further details regarding the uncertainty of Fyw calculation, and references cited in the supporting information

Additional File 2. Table S5. Additional file, 'TableS5.xls', contains full uncertainty calculation per option in Table 1, including all mean and standard deviations of sine wave parameters, young water fraction, mean of determined gamma function parameters alpha and tau and their standard deviations, R^2 values around fit, and whether each was retained in the figures for each site and option.

Additional File 3. 'Fyw.zip'. This file contains a Matlab script to perform all calculations in this manuscript.

Appendix A: Inference of transit time distributions parameter in the convolution approach

We give here details on the classical inverse estimation used for F_{yw} in the convolution approach. The basic principle of inverse estimation is to i) select a parameter set, ii) run the model and repeat i) and ii) until we find the parameters that yield the best fit to the observed output. Transposed to the convolution approach here, this means: i) select a parameter set of the retained transit time distribution, ii) convolve the input signal (equivalent precipitation isotopes) with the transit time distribution and repeat until the resulting output matches closely the streamflow isotopes. The convolution is obtained by multiplication in the Fourier domain.

In case of a Gamma (Γ) distribution, with shape parameter α and location parameter β, the probability distribution reads as

$$h(\tau) = \frac{\tau^{(\alpha-1)}}{\beta^{\alpha}\Gamma(\alpha)} e^{-\frac{\tau}{\beta}}, \quad \text{(A.1)}$$

with mean $\tau = \alpha\beta$. The Fourier transform *H(f)* can be formulated as (Kirchner, 2016a, eq. 7; Walck, 2007):

$$H(f) = (1 - i2\pi f\beta)^{-\alpha}, \quad \text{(A.2)}$$

where *f* is the frequency and $i = \sqrt{-1}$. This formulation of the Fourier transform of the Gamma distribution assumes that the Fourier transform of a function *g(x)* uses the following normalization (Walck, 2007):

$$G(x) = \int e^{-it} g(x) dx. \quad \text{(A.3)}$$

In the direct, forward modeling approach, we convolve the equivalent precipitation isotope signal $C_{Peq}(t)$ with the Gamma distribution by multiplying equation A.2 with a Fast Fourier transform (Matlab 2018) of $C_{Peq}(t)$. We optimize the parameters α, β such that the model output reproduces as closely as possible the observed streamflow isotope composition. We use an objective function *z* that gives more weight to low values to decrease the influence of positive outliers in the streamflow samples during rainfall events:

$$z(\varepsilon) = \sum(\log(x_{\text{obs}} + c) - \log(x_{\text{sim}} + c))^2, \quad \text{(A.4)}$$

where *c* is a small constant offset such that $x_{\text{obs}} > 0$ and $x_{\text{sim}} > 0$.

Details on the optimization algorithm are given in the main text. The Matlab code to perform this is available in the Supplementary Material.

Appendix B: List of abbreviations and variables

ARPAV - Agency for Environmental Protection of Veneto Region
BCC - Bridge Creek Catchment
NBPV - Noce Bianco at Pian Venezia
SCA - snow-covered area
VdN - Vallon de Nant

α - shape factor of the Gamma distribution (Γ)
β - scale factor of the Gamma distribution (Γ)
ζ - degree-day factor [mm/°C/d]
τ - transit time
$\bar{\tau}$ - mean transit time
Γ – Gamma distribution

a – total catchment area
$a_{r,j}$ - area of the non-snow-covered (i.e. receiving rainfall) elevation band *j* and *A* i
$a_{S,i}$ - area of the snow-covered elevation band *i*,
A_P - amplitude of the sine curve fitted to C_P
A_{Peq} - amplitude the sine curve fitted to C_{Peq}
A_Q - amplitude of the sine curve fitted to C_Q
C_P - time-series of precipitation isotopic concentration, general
$C_{P\ -Obs}$ - observed concentration of isotopes in P
C_{P-fit} – sine wave fitted to C_P
C_{P*} - fitted precipitation isotope signal weighted with the simulated amounts of P_{eq}
C_{Peq} - concentration of isotopes in P_{eq}
C_Q- concentration of isotopes in Q, general
C_{Q-Obs} - observed concentration of isotopes in Q
C_{Q-fit} – sine wave fitted to C_Q
C_{Q-Conv}- concentration of isotopes in Q, determined with convolution
C_S - modeled snowpack isotope concentration
F_{yw} - fraction of young water
$F_{yw,Conv}$ - F_{yw} directly from the inferred transit time distribution
$F_{yw,P}$ - F_{yw} equal to the ratio of amplitudes from C_P and C_Q
$F_{yw,P*}$ - F_{yw} based on C_{P*}
$F_{yw,Peq}$ - snowpack modified amplitude ratio approach
H(f) - functional form of the Fourier transform
$h_s(t)$ - snow water equivalent at time t [mm w.e.]
$M(t)$ - daily snowmelt at time t [mm/d]
$P(t)$ - observed daily time-series of precipitation [mm]
P_{eq} - equivalent precipitation [mm]
$P_R(t)$ - rainfall at time t [mm]
$P_s(t)$ - snowfall at time t [mm]
Q - streamflow at outlet of catchment
R^2 - Coefficient of determination
$T(t)$ - observed daily time-series of air temperature
T_0 - air temperature threshold at which snow melts (set to 0) [°C]
T_{crit1} - air temperature threshold below which precipitation falls as snow exclusively [°C]
T_{crit2} - air temperature threshold above which precipitation falls as rain exclusively [°C]
X - streamflow age
x_{yw} - threshold age to define young water

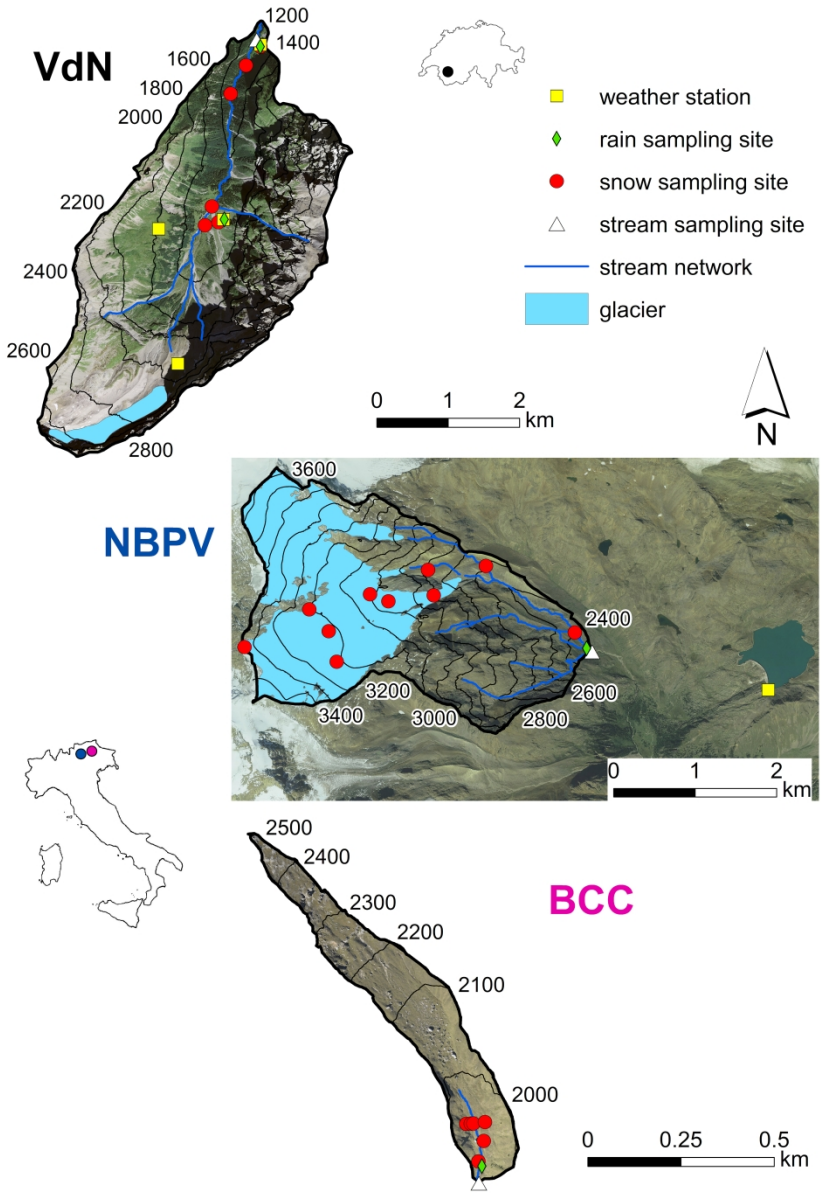

Figure 1. Location of the study catchments in Switzerland and Italy, and position of weather stations and the main sampling sites for rain water, snowpack and stream water. The catchment outlines are shown in black over aerial images, with indication of contour lines.

225x318mm (600 x 600 DPI)

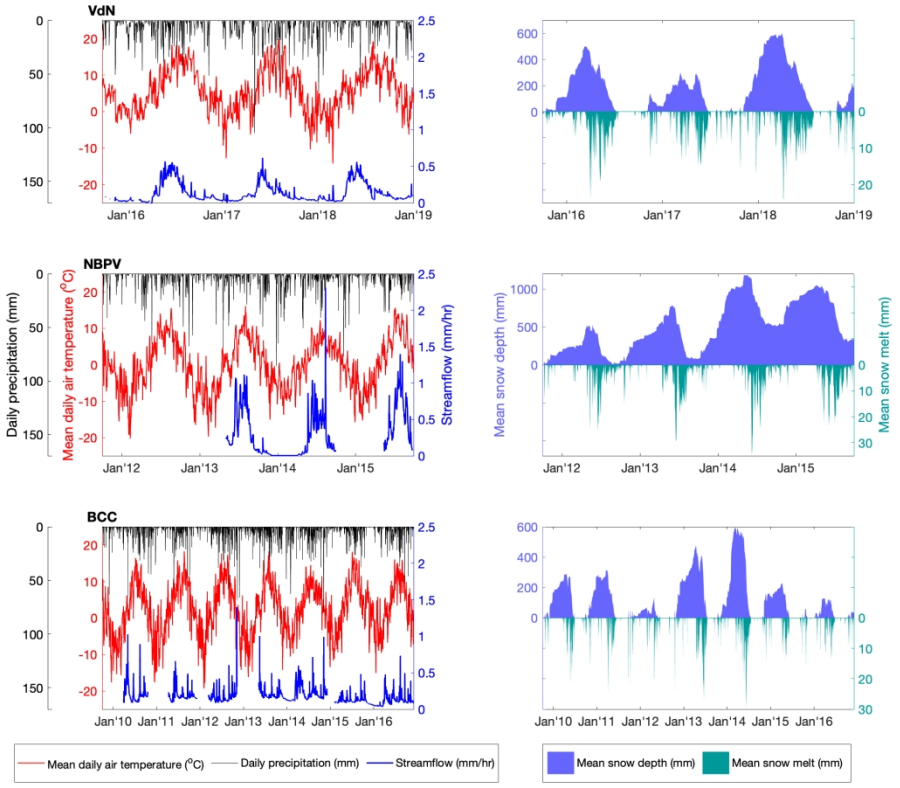

Figure 2: Daily precipitation (second left axis, black), daily mean air temperature (left axis, red), and hourly streamflow (right axis, blue) for the three study catchments in left column. Modeled snow water equivalent shown as mean snow depth, hs (left axis, blue), and snowmelt, M (right axis, cyan) in right column. Note that the scales of the dates and y-axes vary by catchment and variable.

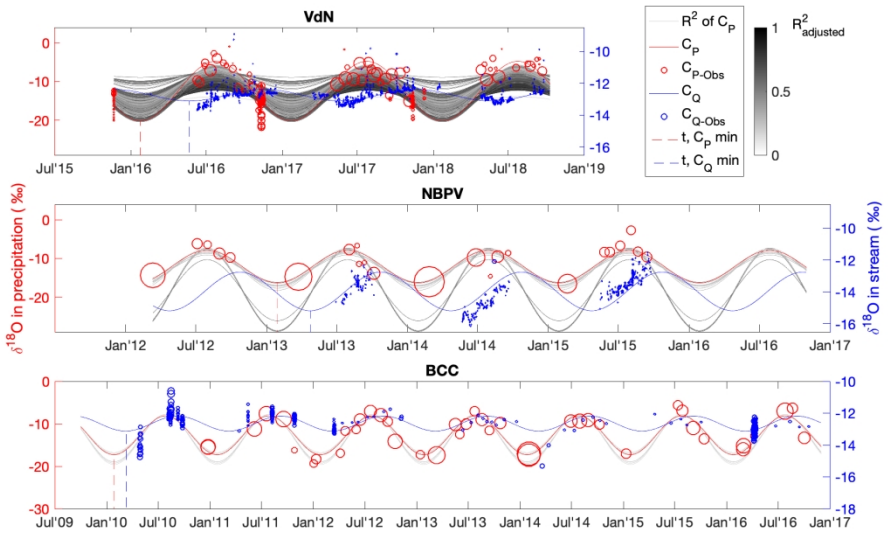

Figure 3: Sine curve fitted to streamflow, Q, and variation in sine wave fitting to precipitation, P, isotopes, for all catchments. Grey scale shows adjusted R^2 for each possible C_P isotope fit. The best fit is highlighted in red; the circles show the used samples for that fit, sized relative to the weight. The best fit corresponds to options 312131 for VdN (R^2=0.88), 121444 for NBPV (R^2=0.90), 115131 for BCC (R^2=0.97) from Table 1. The date of minimum $\delta^{18}O$ in C_Q and C_P (forced by the air temperature) are shown as dashed vertical lines.

714x421mm (72 x 72 DPI)

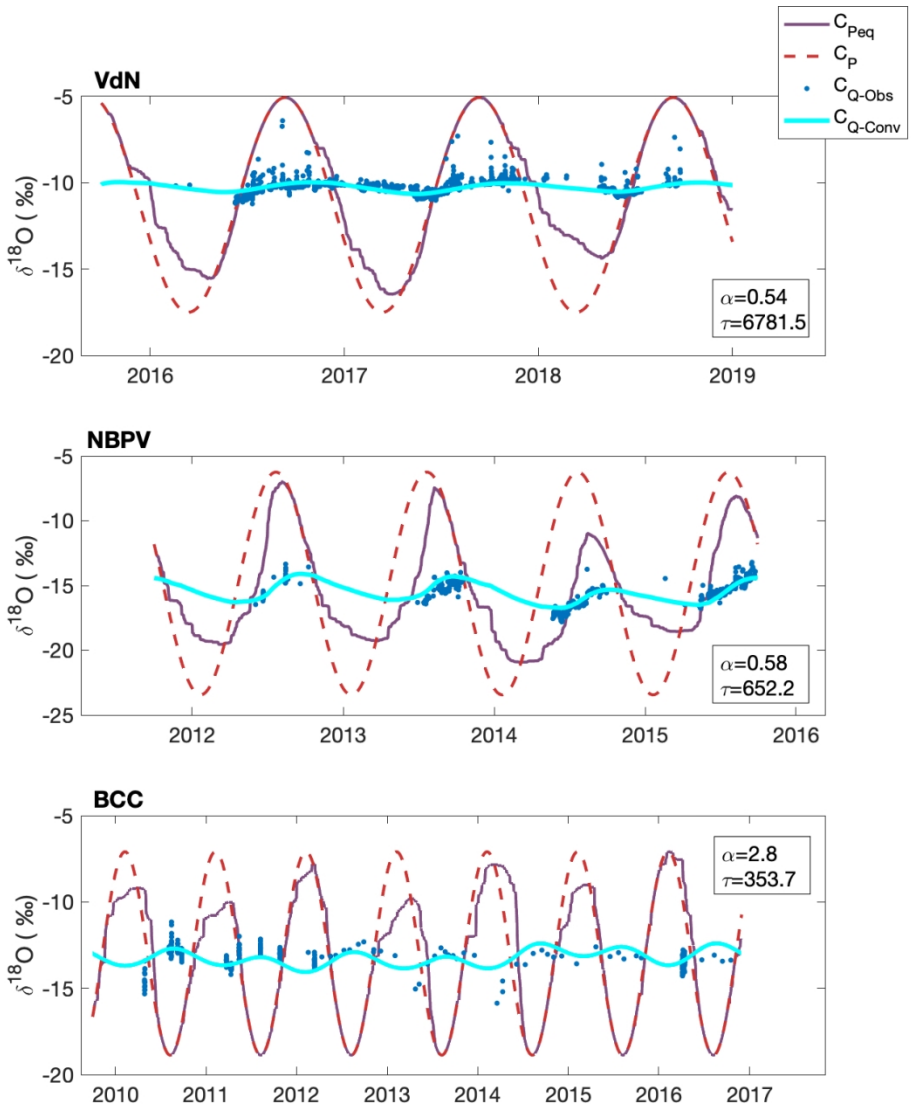

Figure 4. Example of convolution result. Input C_{Peq} isotopes (solid purple line) and isotopes in the output of the convolution ($C_{Q\text{-}Conv}$, solid cyan line), compared with the observations of isotopes in Q ($C_{Q\text{-}Obs}$, blue dots), corrected to the input mean, and the original sine wave of isotopes in P (C_P, dashed red line). The inferred Gamma distribution parameters α and τ for each site are shown. The selected C_P shown here are the same as in Figure 3.

225x281mm (150 x 150 DPI)

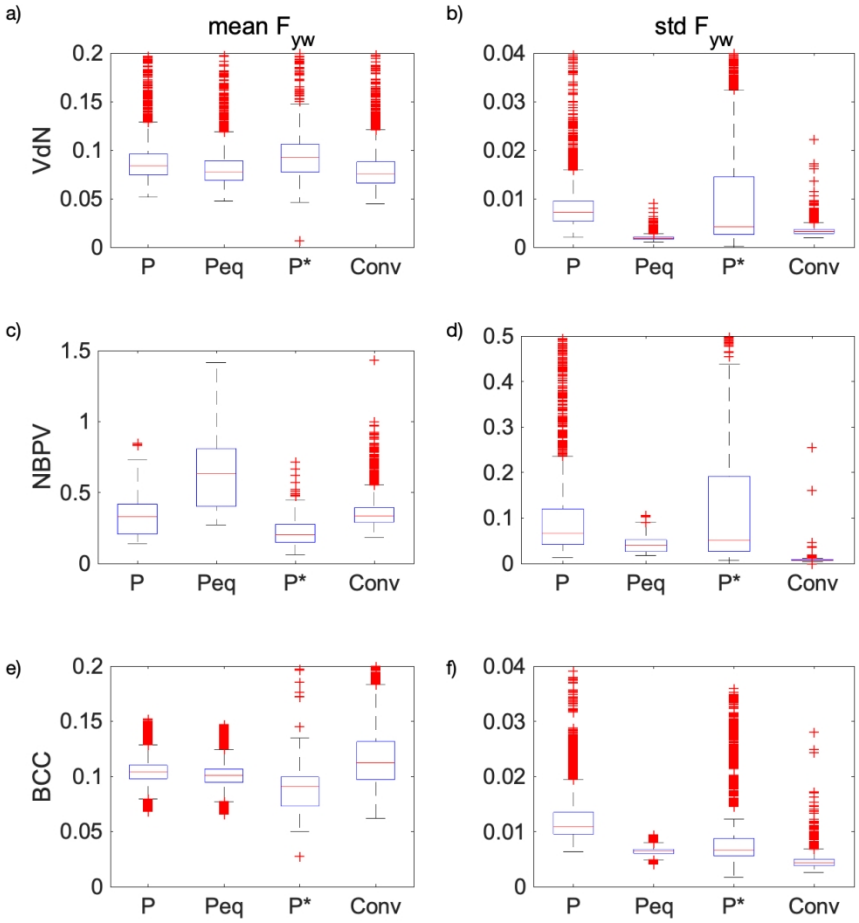

Figure 5: Left column shows the distribution of mean F_{yw} over all time-series construction options for the reduced option range (5600 options, see Table 5) for the three catchments (a, c, e). Right column (b, d, f) shows the distribution of standard deviations around F_{yw} values resulting from Gaussian error propagation corresponding to the time-series construction options and catchments as in left column. F_{yw} values computed with the convolution approach (Conv, right most boxes) show standard deviations estimated from the posterior distributions of the Gamma parameters α and β.

509x537mm (72 x 72 DPI)

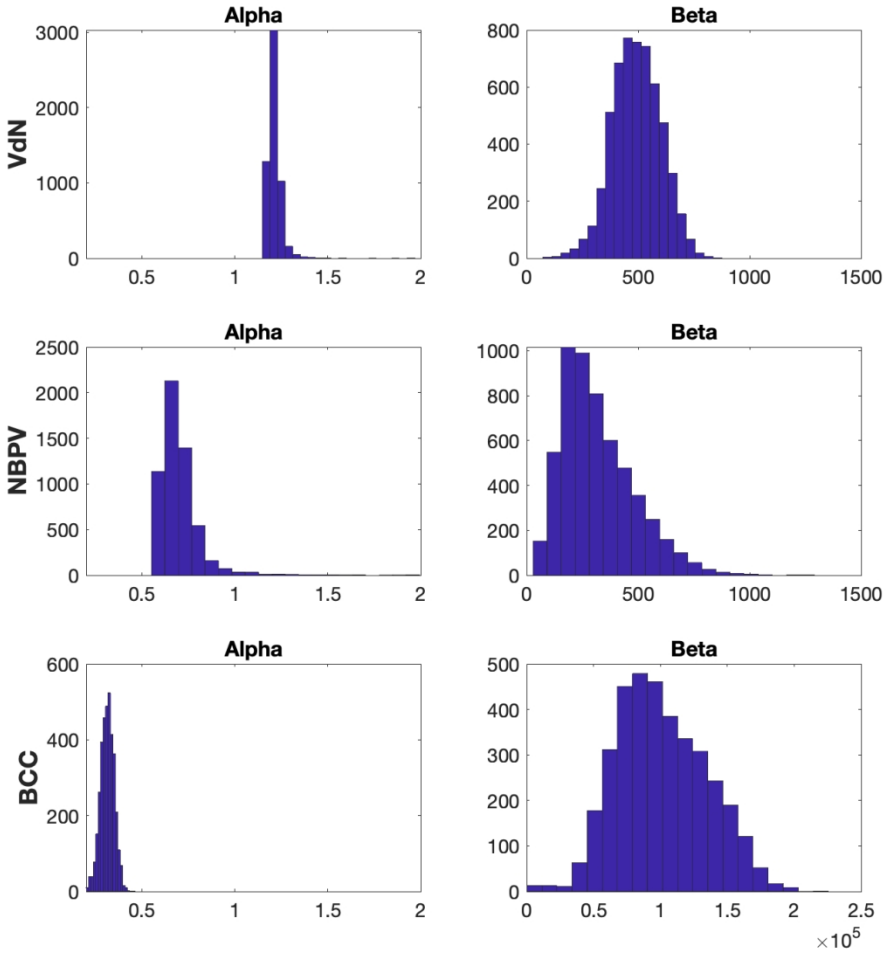

Figure 6.Distribution of median Gamma parameters per time-series construction option for the reduced option range (5600 options, see Table 5). Left column shows α and right column beta (β), and rows show the three sites, VdN, NBPV, and BCC.

509x537mm (72 x 72 DPI)

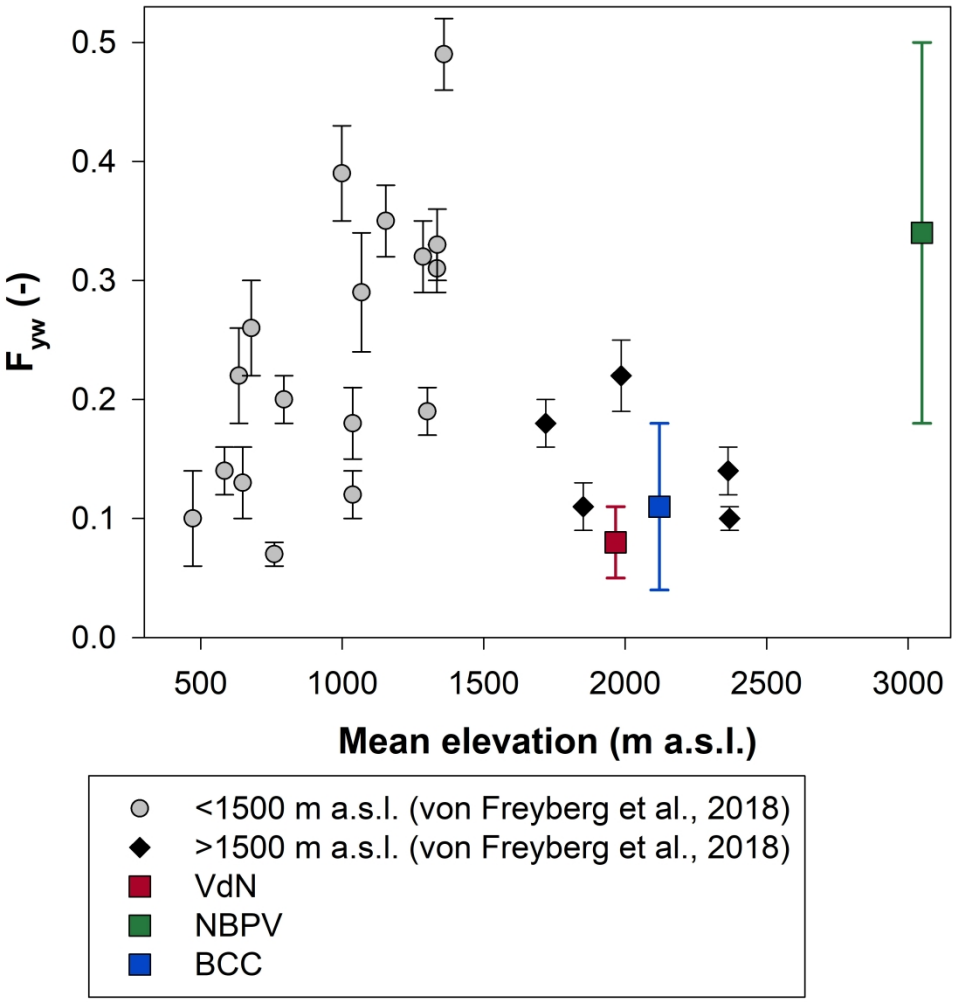

Figure 7. Relation between F_{yw} and mean elevation for 22 Swiss catchments (grey circles sites < 1500 m. a.s.l. and black diamonds sites >1500 m. a.s.l., von Freyberg et al., 2018) and our three sites. Colored squares are F_{yw} from the theoretical amplitude dampening (application of eq. 8 of Kirchner, 2016a) with the inferred Gamma distribution, with error bars showing the standard deviation.

173x187mm (600 x 600 DPI)

Supporting information for: Seasonal snow cover decreases young water fractions in high Alpine catchments

Natalie Ceperley[1,2,3], Giulia Zuecco[4], Harsh Beria[1], Luca Carturan[4,5], Anthony Michelon[1], Daniele Penna[6], Joshua Larsen[1,7,8], Bettina Schaefli[1,2,3]

[1]Institute of Earth Surface Dynamics, University of Lausanne, Lausanne, Switzerland
[2] Now at: Institute of Geography, University of Bern, Bern, Switzerland
[3]Now at: Oeschger Centre for Climate Change Research, University of Bern, Bern, Switzerland
[4]Department of Land, Environment, Agriculture and Forestry, University of Padova, Italy
[5]Department of Geosciences, University of Padova, Italy
[6]Department of Agriculture, Food, Environment and Forestry, University of Florence, Italy
[7] Now at: School of Geography, Earth and Environmental Sciences, University of Birmingham, United Kingdom
[8] Now at: The Birmingham Institute of Forest Research (BIFoR), University of Birmingham, United Kingdom

Correspondence to:

Natalie Ceperley, natalie.ceperley@giub.unibe.ch, Institute of Geography, University of Bern Hallerstrasse 12, 3012 Bern, Switzerland

Content

This supporting information contains additional details regarding study sites and datasets including flow duration curves and sample size (Section S1) and details of snowpack determination and validation (Section S2). Section S3 presents the distributions and mean values of all fitted sine curves. Finally, it contains further details regarding the uncertainty, S4. A final section explains Table S5, which is an accompanying spread sheet, and the accompanying code (in Matlab format).

S1 Additional details regarding study catchments and datasets

This section includes additional details on study sites and datasets, the sample size (Table S1) and a Figure showing the distribution of isotopes according to the flow duration curves (Figure S1).

S1.1 Additional details regarding Vallon de Nant (VdN)

Data from the Swiss automatic meteorological station network is used to gap fill the local observations (i.e., 12 missing days in 2017). A total of 135 bulk rain samples were collected using funnels flowing into insulated bags at three locations corresponding to the rain gauges (at 1253, 1500, and 2100 m a.s.l.), and emptied weekly or biweekly between June 2016 and November 2018. Between February 2016 and April 2018, 199 snow samples were collected from the entire snow profile at various locations in the catchment (Figure 1).

Snow-covered area (SCA) was calculated as a ratio from 0 to 1 over the non-forested part of the catchment using 21 Landsat 8 images, and 24 Sentinel 2 images retrieved between September 2016 and December 2017 (Michelon, Ceperley, Beria, Larsen, & Schaefli, 2018). A linear interpolation of the combined time-series was used to provide a fractional SCA per sampling date. A stream gauging station in the Avançon defines the catchment of the VdN (Figure 1).

S1.2 Additional details regarding Bridge Creek Catchment (BCC)

BCC is a soil-mantled catchment with steep hillslopes, a distinct riparian zone (Penna, van Meerveld, Zuecco, Fontana, & Borga, 2016) and saturated areas. Cambisols with mull are the main soil types; soil texture is dominated by clay (range of 45-73% in the soil profile) and has a small fraction of silt (16-28%) and sand (3-25%).

Table S1 Sample size according to catchment.

Total counts	**VdN**	**NBPV**	**BCC**
Precipitation samples (rain + snow)	314	45	81
Stream samples	1676	485	346

S2 Snowpack simulation

This section contains details regarding the snowpack simulation (S2.1), figures showing its validation (Figure S2), and the sensitivity of the $F_{yw,conv}$ calculation to it (Figure S3).

S2.1 Specific decisions regarding temperature thresholds and their determination, degree-day factors, subsequent sensitivity analysis

Given that relatively few observations were available for the calibration of the snow model, we tested the sensitivity of F_{yw} calculated from the Gamma parameters, α and τ, to different sets of values for the minimum (T_{crit1}) and maximum (T_{crit2}) temperature thresholds for precipitation falling as snow and degree-day (ζ) factors (Figure S3). This sensitivity analysis shows that the snow parameters have little effect on the F_{yw} for VdN and BCC but important effects on NBPV, particularly for ζ below 2°C.

S3 Details on fitted sine curve parameters

This section contains tables showing additional sine fit parameters (amplitude is in the main text, Table 4), adjusted R^2 (Table S2), mean values (Table S3), and phases (Table S4).

Table S2: Adjusted R^2 for sine curve fitting to discharge (no options) and for all possible precipitation time-series construction options ('all', 6720 options) and for reduced range of options, excluding the option to set the snowpack date stamp to the day of collection ('red', 5600 options); for NBPV, we also removed all options that lead to $R^2<0$ for precipitation sine curve fits (corresponding to 325 removed options); for equivalent precipitation, R^2 is close to 1 for all options.

		VdN			NBPV			BCC		
		Min	**Max**	**Median**	**Min**	**Max**	**Median**	**Min**	**Max**	**Median**
all	***Q***	-	-	0.84		-	0.58	-	-	0.81
	P	0.27	0.88	0.64	-0.23	0.90	0.50	0.26	0.97	0.78
	P*	0.02	0.99	0.77	-0.15	0.86	0.66	0.40	0.99	0.89
red	***Q***	-	-	0.84	-	-	0.58	-	-	0.81
	P	0.27	0.86	0.63	0.00	0.90	0.51	0.26	0.95	0.77
	P*	0.02	0.99	0.77	0.01	0.86	0.70	0.40	0.99	0.89

Table S3: Mean values of the fitted sine curves for *Q, P*, *Peq* and $P^*(\delta^{18}O \text{ in } ‰)$. For precipitation, all possible precipitation time-series construction options, except setting the snowpack date stamp to the day of collection (total of 5600 options); for NBPV, we also removed all options that lead to adjusted $R^2<0$ for precipitation sine curve fits (corresponding to 338 removed options). For VdN, 8 options lead for P^* to a strong weighting of a few samples and ensuing high amplitude (57.84) and upward shift of the entire sine curve (mean 38.84), which were not removed but explain the extremely high maxiums.

	VdN				NBPV				BCC			
	Min	**Max**	**Median**	**Std**	**Min**	**Max**	**Median**	**Std**	**Min**	**Max**	**Median**	**Std**
Q	-	-	-12.8	0	-	-	-14.6	0	-	-	-12.7	0
P	-13.4	-8.7	-11.6	0.6	-18.8	-10.6	-13	1.81	-14.0	-11.6	-12.8	0.6
Peq	-13.7	-8.8	-12.2	0.6	-19.4	-10.8	-13.3	1.92	-15.7	-12.0	-13.3	0.6
P*	-16.0	38.9	-10.5	2.9	-28.5	8.5	-13.9	4.2	-22.1	-8.9	-13.56	1.7

Table S4: Phase of the fitted sine curves for *Q, P*, *Peq* and P^*. For precipitation, the phase is forced to follow the air temperature cycle, indicated by *fix*; accordingly, sine curves fitted to the modelled Peq (having the precipitation sine curve as input) also have an almost constant phase. All values are in days.

	VdN				**NBPV**				**BCC**			
	Min	**Max**	**Median**	**Std**	**Min**	**Max**	**Median**	**Std**	**Min**	**Max**	**Median**	**Std**
Q	-	-	245	0	-	-	179	0	-	-	145	0
P	-	-	116	0	-	-	122	0	-	-	119	0
Peq	-	-	122	0	-	-	159	0	-	-	134	0
P^*	12	204	113	18	75	354	109	53	102	228	118	14

S4 Uncertainty of F_{yw} calculation

This section contains figures showing further information regarding the uncertainty calculation, including the effect of construction of precipitation isotope series on F_{yw} (Figure S4), histograms of the mean F_{yw} determination (Figure S5), distribution of the standard deviations of the gamma parameters (Figure S6), and as an additional file, a spreadsheet showing the full uncertainty calculation (Table S5).

S5 Additional Files

Additional file, 'TableS5.xls', contains full uncertainty calculation per option in Table 1, including all mean and standard deviations of sine wave parameters, F_{yw}, mean of determined gamma function parameters α and τ and their standard deviations, R^2 of fit, and whether each was retained in the figures for each site and option.

Additional file, Fyw.zip, contains a Matlab script to perform all calculations in this manuscript.

References

Michelon, A., Ceperley, N., Beria, H., Larsen, J., & Schaefli, B. (2018, April). *Quantification of snowmelt processes in a high Alpine catchment from hydrographs and satellite images and stable water isotopes.* Paper presented at the European Geophysics Union General Assembly.

Penna, D., van Meerveld, H. J., Zuecco, G., Fontana, G. D., & Borga, M. (2016). Hydrological response of an Alpine catchment to rainfall and snowmelt events. *Journal of Hydrology, 537*, 382-397. doi:10.1016/j.jhydrol.2016.03.040

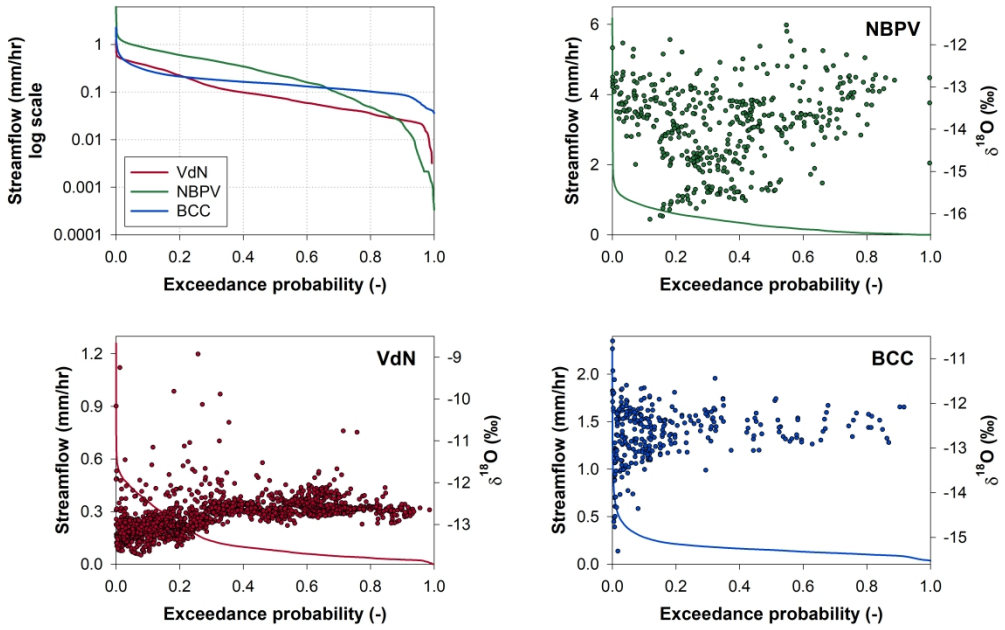

Figure S1. Flow duration curves for each study catchment. Isotope concentrations of individual samples are plotted according to the exceedance probability of the streamflow at the moment they were sampled.

393x257mm (300 x 300 DPI)

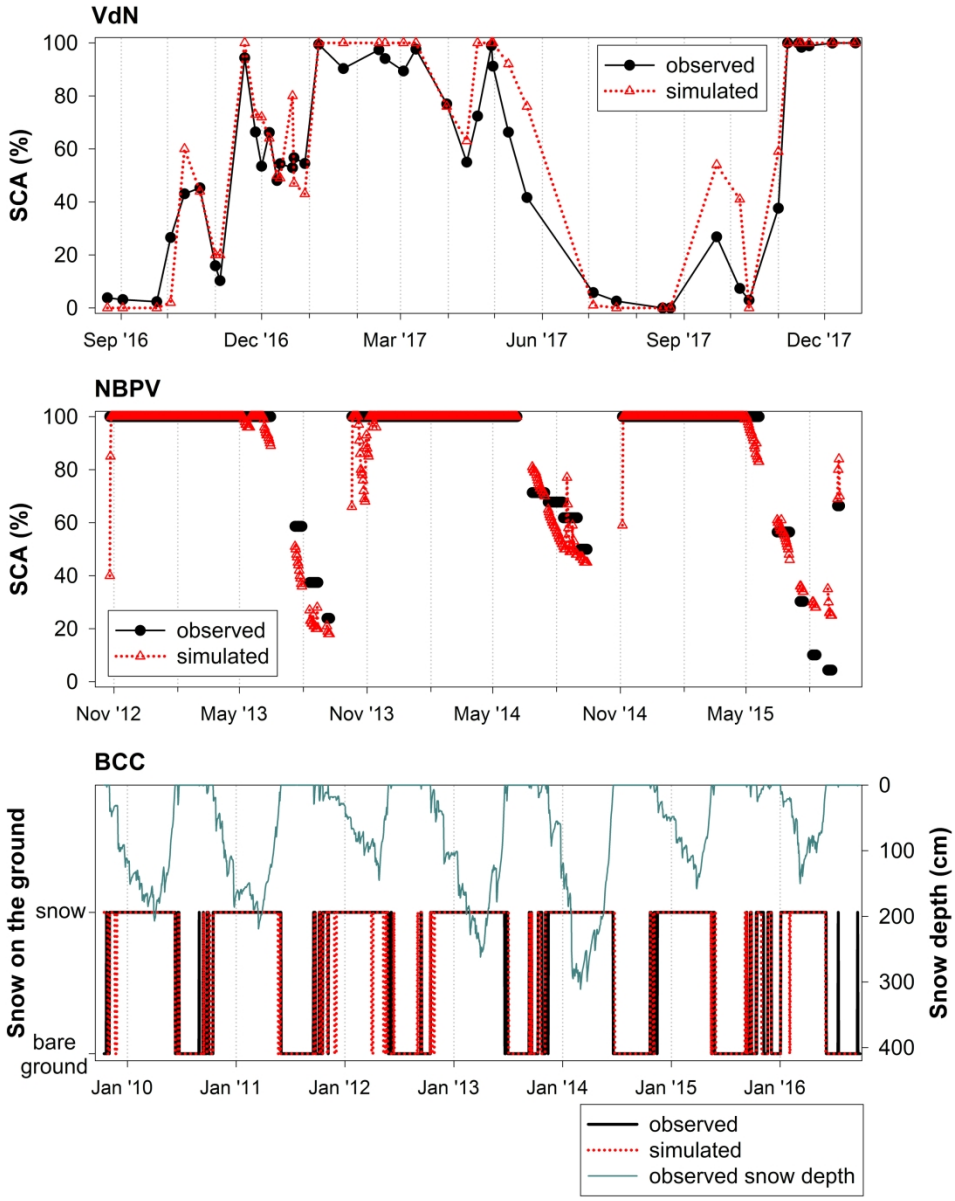

Figure S2. Snowpack validation in two sites (VdN and NBPV) based on snow covered area (SCA) extracted from satellite data (solid black line with circles). The snowpack simulation in the third site (BCC) was done with snow depth measurements but only differentiated whether there was snow or not.

236x296mm (300 x 300 DPI)

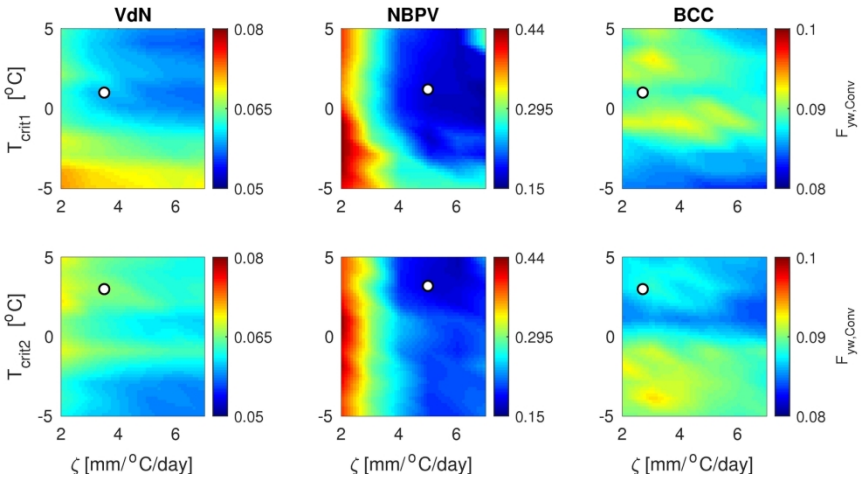

Figure S3. Subplots showing effect of snowpack parameters on the young water fraction ($F_{yw,Conv}$). In all subplots, the x-axis shows the degree day factor (ζ). The first row shows the effect of varying the minimum critical temperature (T_{crit1}), above which precipitation no longer falls exclusively as snow, the second row shows the effect of varying the maximum critical temperature (T_{crit2}), above which precipitation always falls as rain. The color axis shows the $F_{yw,Conv}$. The columns are the different sites. The black circles show the parameters selected with the snowpack validation.

207x99mm (300 x 300 DPI)

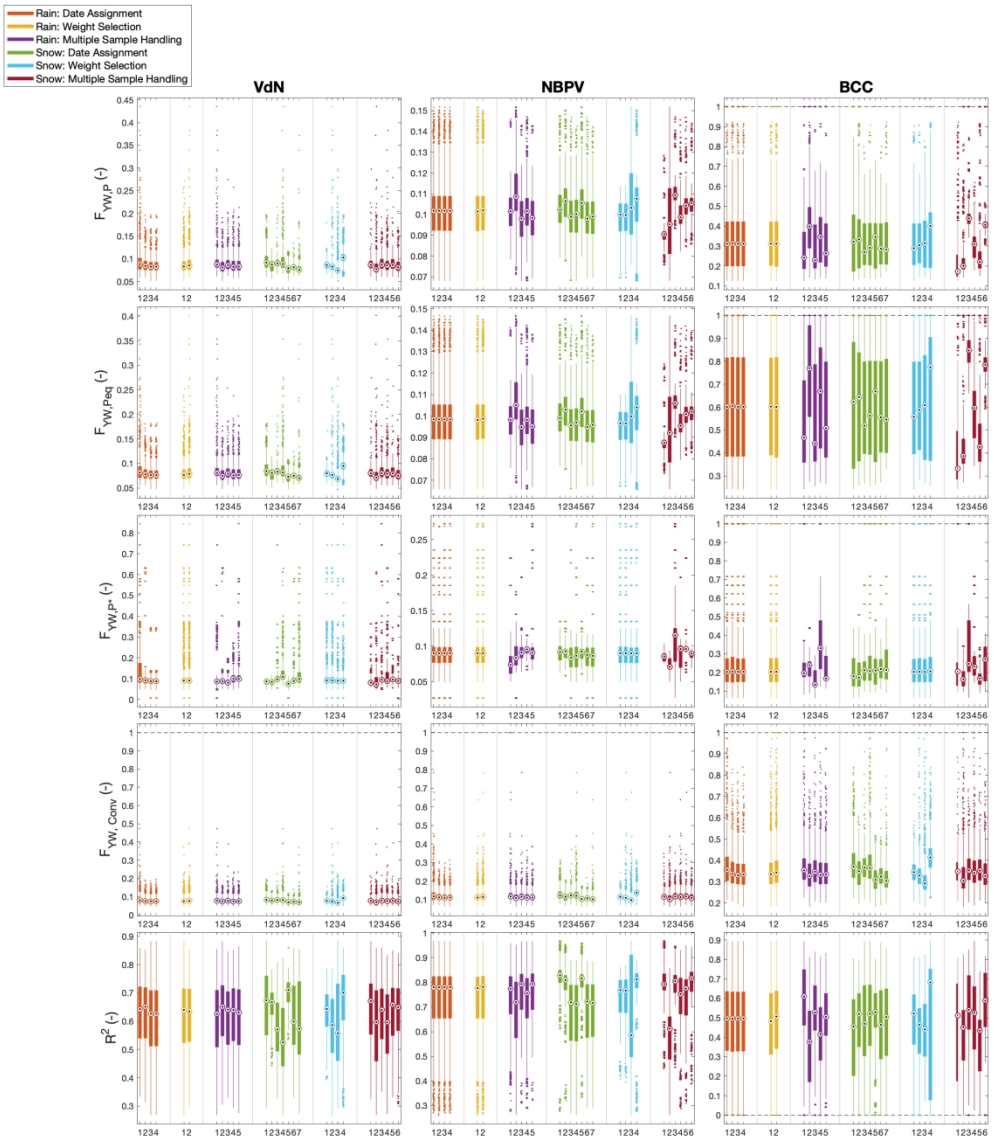

Figure S4. Boxplots showing the effect of choices (colors) for construction of time-series of precipitation on final $F_{yw,Conv}$ determined according to 4 methods (rows) at 3 sites (columns). Final row shows the adjusted R^2. Numbers (along x-axes) and names (legend) correspond to Table 1. In each box, the central dot indicates the median, edges of the solid box indicate the range of the 25th to 75th percentiles, whiskers extend to the most extreme data points and outliers are shown as open circles.

406x461mm (300 x 300 DPI)

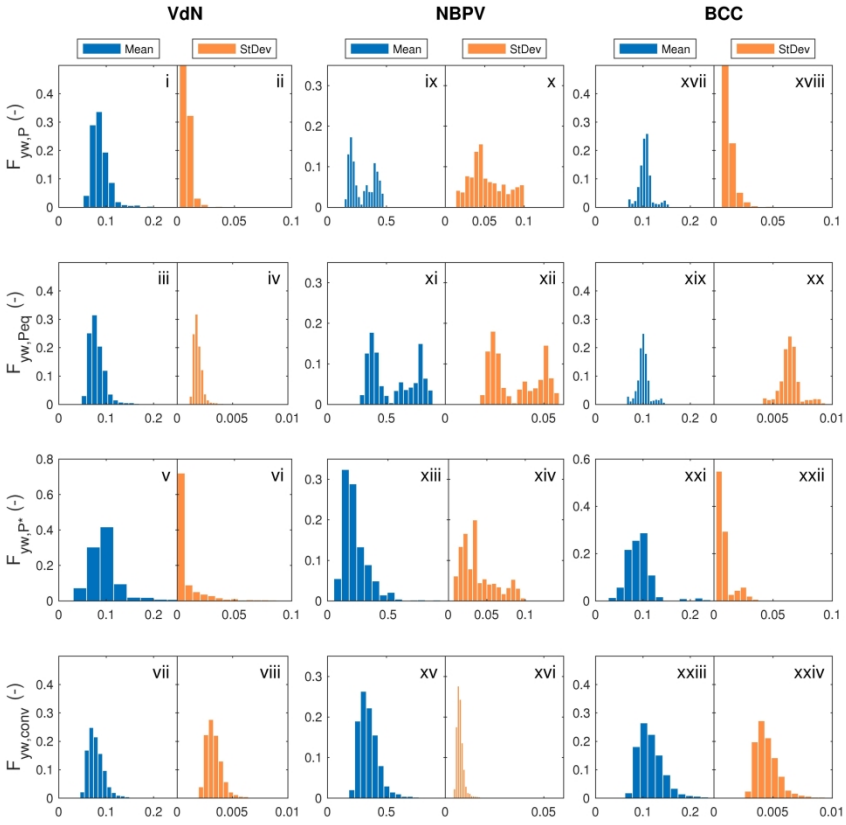

Figure S5: For each case study, the left (blue) plot shows the distribution of the mean and the right (orange) plot, shows the distribution of the standard deviation. The full range of values for all samples can be seen in the separate file, 'TableS5.xls'. The standard deviation shows the standard deviation per option, not the standard deviation across the options.

275x246mm (300 x 300 DPI)

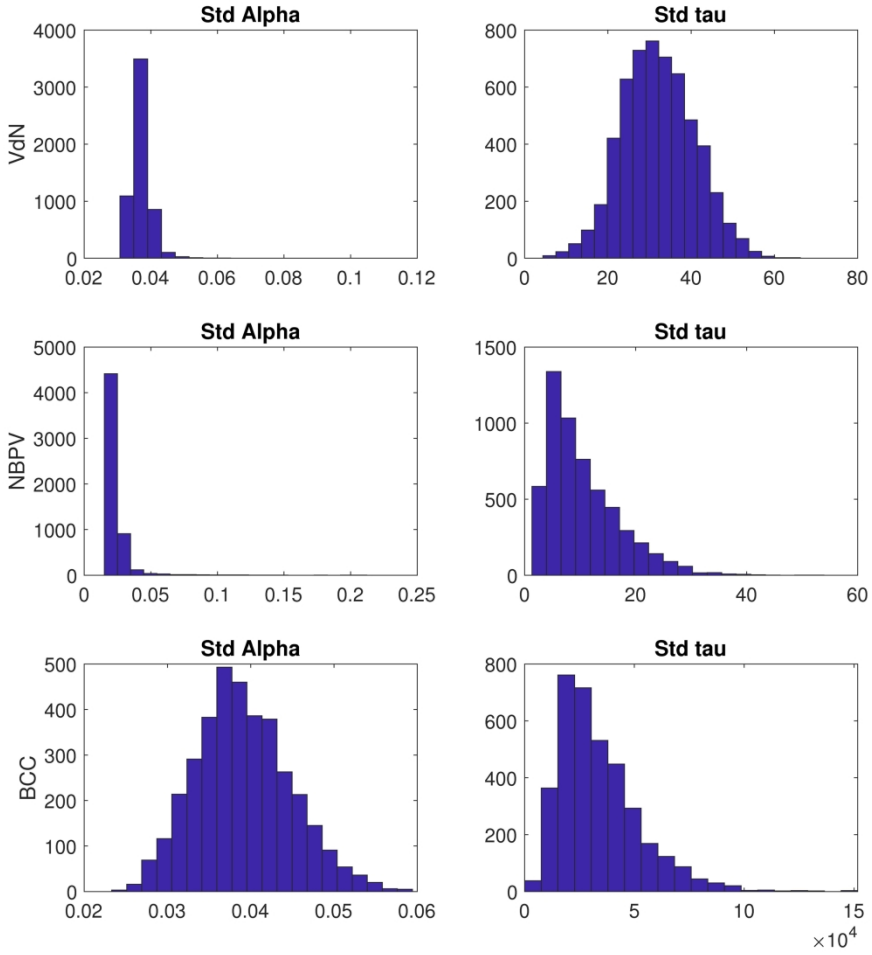

Figure S6: Distribution of standard deviations of Gamma parameters in the convolution approach ($F_{yw,Conv}$); shown is the distribution of tau (τ) and not β=τ/α since we inferred τ and not beta in the Matlab implementation.

254x268mm (300 x 300 DPI)

Tuesday, October 6, 2020

Dear Paolo Benettin,

We would like to thank you for the work you have done editing and working with reviewers to improve our article. Thank you for acknowledging and appreciating the work we did revising the manuscript. Below is a summary of the changes made according to the final comments by reviewer 1. There were no comments from the editor or the other 2 reviewers. We have also listed other changes below for consistency.

Thank you for accepting our revised manuscript for publication in Hydrological Processes,

Natalie Ceperley on behalf of the authors

Reviewer 1 Comments:

1. In various places throughout the manuscript, the estimated young water fractions are compared with those obtained by von Freyberg et al. (2018). The definition of Fyw used by von Freyberg is, however, quite different from the one in this manuscript (and this is precisely the point of the manuscript presented here). While von Freyberg define young water fractions as the time water takes from entering the catchment as precipitation (no matter whether this is rain or snow) to leaving it as streamflow, the presented manuscript quantifies the time between the liquid water input (rain or snow melt) to streamflow. Both definitions are of course valid, but this difference has implications for the expected values of Fyw, but it is not pointed out explicitly in the manuscript. A suitable place to do so could be at the end of the introduction, for example.
    - We added a sentence clarifying the definition to last paragraph of the introduction: “Moreover, our approach removes the potential confusion associated with defining the input timing as being whenever precipitation falls, regardless of the phase (snow or rain) (von Freyberg et al., 2018).”

2. The authors have added important site information to the revised manuscript, only at NBPV they seem to have forgotten to provide the elevation range.
    - The elevation range is in Table 2, but additionally we have added it to the site description: “with an elevation that ranges from 2298 to 3769 m a.s.l..”

3. It would also be helpful to know how the precipitation samples from the three different bulk rain sampling stations at VdN were aggregated to the final precipitation isotope value used for further analysis.

- This is explained according to the options in Table 1. Aggregation is described in the two columns, one for rain and one for snow, titled "Multiple sampling handling". Different options aggregated them differently.
- We have pointed this out in the site description as well: "Aggregation of these samples occurred according to various options presented subsequently."

4. I am also slightly concerned that most of the precipitation (rate and isotope) measurements were done in the lower sections of the catchments, or even at the outlet, and no altitude correction was applied. I understand that sampling and measurements at higher elevations are often not feasible, but this limitation should be pointed out in the text.

- We have pointed out why no isotope adjustments were made: "From available data at the studied catchments (see Sections 3.1, 3.2, and 3.3.) and nearby sites, no consistent lapse rate in isotopic composition in either rain or snow could be established (Zuecco, Carturan, et al., 2019), thus none is implemented here."
- We have also added the sentence (to Section 5.2): "In an ideal scenario, if field conditions permitted year-round, exhaustive sampling, observations would be made at adequately high spatial and temporal resolutions that the natural variation would be overcome by obvious physical and temporal signatures.".

5. The list of abbreviations at the end is certainly helpful. The way the manuscript is written, however, readers are forced to turn to this table quite frequently. It would be great if the authors could explicitly describe the entity represented by the variable. For example, in line 398, the authors write "…jointly with ζ." Why not write "…jointly with the degree factor, ζ." instead? I understand that the authors are very familiar with the variables and their meaning, but the readers may not be.

- Thank you for this suggestion. We have modified this sentence (2.1.3): "The snowpack model has three case-study specific parameters: T_{crit1} and T_{crit2}, the lower and upper thresholds, for snowfall occurrence and ζ, the degree-day factor for snowmelt."
- And later (4.1): "The snowfall thresholds T_{crit1} and T_{crit2} from Equation (1) were previously determined experimentally for NBPV (Carturan et al., 2019); for the other two study sites, they are calibrated based on the available snow cover area (SCA) or snow cover duration observations (Table 3 and Figure S2), jointly with the degree-day factor ζ."

Specific comments:

6. Line 28: "Fyw is 3-4 times greater", greater compared to what?
   - Thank you for pointing out that this is not clear, we have added precision (abstract): "In contrast, in the highest elevation, glacier dominated

catchment, F_{yw} is 3-4 times greater compared to the other two catchments, due to the lower storage and faster drainage processes."

7. Line 418: I think this should be +0.23, rather than -0.23 (R2 value).
   - No, this is correct. It can be negative because it is an adjusted R2 value.

Additional Changes:

1. The Matlab and excel files have been sent to the editor for direct upload as part of the main supporting information, so the additional supporting information file on Github will be deleted.

2. Affiliations have been updated. There is some confusion as to how to clearly list multiple affiliations. For three authors it is necessary to list a university where the bulk of this work took place as a main affiliation but indicate that they are now at 2 new affiliations. Thus, the editorial assistant's wish (communicated via email) to "please include only the latest institution", was not possible.

3. There is a slight word order change in the title:

   Young water fractions instead of fraction of young water

4. The abstract and conclusion have been reworked slightly to improve readability.

5. Some words have been modified for consistency.

6. In Section 5.3, we have added a reference to the most resent Fyw paper: "Similarly, our are consistent with the spread of F_{yw} (7-23%) for a catchment in the Canadian Rockies ranging in elevation from 1200 to 3500 m. a.s.l. (Campbell, Pavlovskii, & Ryan, 2020)."

7. All internal links were removed but the doi's in the reference list were verified and maintained with hyperlink whenever possible, as per the editorial assistant's wishes.